A MICRO-ASPIRATOR CHIP USING VACUUM EXPANDED MICROCHANNELS FOR HIGH-THROUGHPUT MECHANICAL CHARACTERIZATION OF BIOLOGICAL CELLS

A Thesis

by

WOOSIK KIM

Submitted to the Office of Graduate Studies of
Texas A&M University
in partial fulfillment of the requirements for the degree of

MASTER OF SCIENCE

August 2010

Major Subject: Biomedical Engineering

A MICRO-ASPIRATOR CHIP USING VACUUM EXPANDED MICROCHANNELS FOR HIGH-THROUGHPUT MECHANICAL CHARACTERIZATION OF BIOLOGICAL CELLS

A Thesis

by

WOOSIK KIM

Submitted to the Office of Graduate Studies of
Texas A&M University
in partial fulfillment of the requirements for the degree of

MASTER OF SCIENCE

Approved by:

Chair of Committee,	Arum Han
Committee Members,	Roland R. Kaunas
	Jun Kameoka
Head of Department,	Gerard L. Cote

August 2010

Major Subject: Biomedical Engineering

ABSTRACT

A Micro-aspirator Chip Using Vacuum Expanded Microchannels for High-throughput Mechanical Characterization of Biological Cells. (August 2010)

Woosik Kim, B.S., Seoul National University

Chair of Advisory Committee: Dr. Arum Han

This thesis presents the development of a micro-aspirator chip using vacuum expanded microchannels for mechanical characterization of single cells. Mechanical properties of cells can offer valuable insights into the pathogenic basis of diseases and can serve as a biomarker to identify cells depending on disease state, and thus have the potential for use in human disease diagnostic applications.

Micropipette aspiration and atomic force microscopy (AFM) are the most commonly used techniques for measuring mechanical properties of single cells. Though powerful and versatile, both methods have two drawbacks. First, micromanipulation of glass micropipettes and AFM tips require expertise and extensive operator skills. Second, the serial manipulation process severely limits the throughput. Although recently reported microfluidic micropipette device showed the potential of microfluidic chip type micropipette aspiration, difficulty in cell trapping and unnatural cell deformation remain to be solved.

In order to address these limitations, a high-throughput micro-aspirator chip, which can deliver, trap, and deform multiple cells simultaneously with single-cell

resolution without skill-dependent micromanipulation was developed. The micro-aspirator chip is composed of 20 arrays of cell traps and aspiration channels. The principle of cell trapping is based on differences in flow resistance inside the microfluidic channels. Once the first cell trap is filled with a cell, the next cell coming in passes by the trap and is captured in the next trap. After all traps are filled with cells, negative pressure can then be applied to the integrated aspiration channels using hydrostatic pressure. The aspiration channels are positioned at the center of a trapped cell both in vertical and horizontal directions to obtain a good seal just like a traditional micropipette, a design made possible through a vacuum expanded raised microfluidic channel fabrication technique.

Device operation was demonstrated using HeLa cells. The cell trapping efficiency was almost 100%. Using this device, Young's modulus of 1.3 ± 0.8 kPa (n = 54) was obtained for HeLa cells. Device to device variation was less than 15.2% (n = 3), showing good repeatability of the device. No dependence of the Young's modulus on the cell diameter was found.

DEDICATION

I dedicate this thesis to my parents who have supported my educational upbringing throughout my life.

ACKNOWLEDGEMENTS

I would like to express my sincerest gratitude to all who directly and indirectly have been instrumental in helping me complete this thesis. Especially, I would like to thank my committee chair, Dr. Arum Han, and my committee members, Dr. Roland Kaunas and Dr. Jun Kameoka, for their guidance and support throughout the course of this research.

Thanks also go to my friends and colleagues and the department faculty and staff for making my time at Texas A&M University a great experience.

Finally, thanks to my mother and father for their patience and love and to my supporter for the endless encouragement.

NOMENCLATURE

μTAS	Micro-Total Analysis System
PDMS	Poly (Di-Methyl) Siloxane
AFM	Atomic Force Microscope
SEM	Scanning Electron Microscope
RPM	Rotations Per Minute
CAD	Computer Aided Design
Re	Reynolds Number
UV	Ultra-Violet
PR	Photo Resist
IPA	Isopropyl Alcohol
PBS	Phosphate Buffered Saline
DMEM	Dulbecco's Modified Eagle Medium
BS	Bovine Serum
MEMS	MicroElectroMechanical Systems

TABLE OF CONTENTS

CHAPTER Page

LIST OF FIGURES

Page

Page

Page

LIST OF TABLES

Page

CHAPTER I

INTRODUCTION

1.1 Objective and Motivation

The objective of this work is to develop and demonstrate a system for high-throughput measurement of mechanical properties of single cells. The research focuses in particular on hydrodynamic cell trapping and microfluidic aspiration of single cells using a microfluidic chip, as well as developing fabrication techniques to make raised microfluidic aspiration channels for efficient aspiration of single cells into the aspiration channel.

Micropipette aspiration is the most simple and direct method for studying mechanical properties of a single cell [1]. This technique uses suction pressure to partially or wholly suck a single cell into a glass micropipette and uses microscopy to record the shape change of the cell. By measuring the cell elongation length into the pipette as a result of the suction pressure, mechanical properties of the cell can be evaluated. Currently available systems require laborintensive manual operation that limits the throughput of such systems. Micromanipulation of glass micropipettes requires expertise and extensive operating skills, and the serial manipulation process severely limits the throughput.

Recently, microfluidic devices have been widely used for studying cell biology

---

This thesis follows the style of *IEEE Transactions on Electron Devices*.

since its scale of size is well matched to the physical dimensions of most cells, and micron-scale tools make it possible to manipulate individual cells, their immediate extracellular environments and ultimately, their shape and internal organization [2]. Among various microfabrication techniques, soft lithography is being used with increasing frequency for the fabrication of microfluidic devices because of their simplicity, low cost and compatibility with cells [3]. Previous studies show that flow-through type microfluidic devices can be used to distinguish stiffness difference of single cells depending on the stage of disease but they were not designed to provide absolute value of stiffness [4-6]. Microfluidic micropipette device which can deform and measure the stiffness of four cells simultaneously was reported in 2007 [7]. Although this study showed the potential of microfluidic micropipette device for high-throughput characterization of single cells, it was difficult to obtain a good seal between the cell and the aspiration channel, which is critical for accurate measurement of pressure in micropipette aspiration, due to the location of the aspiration channel lying on the bottom of the device.

A micro-aspirator chip that can deliver, trap, and deform 20 cells simultaneously with single-cell resolution without skill-dependent micromanipulation was designed and fabricated using microfabrication techniques including photolithography and soft lithography. One of the key design concepts of this device is that the aspiration channel is positioned at the center of the cell both in vertical and horizontal directions to obtain a good seal just like a traditional micropipette. The developed system is expected to eliminate the labor-intensive nature of conventional micropipette aspiration, enable fast

and accurate characterization of single cells through cell trapping using flow resistance inside microchannel and cell deforming using hydrostatic pressure, and achieve high throughput measurement of stiffness. By realizing micropipette aspiration into a chip-based system, the developed micro-aspirator chip is expected to provide an in-depth look at mechanical deformation occurring at the single-cell level and pathological status of single cells with high throughput. The result of this study is expected to be applied for high-throughput single cell study and human disease diagnosis such as cancer by providing an accurate and effective analysis instrument.

1.2 Mechanical Properties of Cells and Human Disease

Human disease can be defined as a condition, state or process occurring in our body that not only impairs our bodily structures and functions but also threatens our health and even lives. According to a study by the World Health Organization (WHO) [8], 7.9 million people worldwide died of cancer during 2007 alone. WHO estimates that mortality rates due to cancer will continue to rise worldwide, with 9 million cancer deaths by 2015 and 11.4 million by 2030. Half of the world's population is at risk of malaria, and an estimated 243 million cases led to an estimated 863,000 deaths in 2008 [9]. Every disease is unique and can vary in symptoms, signs and outcomes. Disease not only causes biological and functional alterations but also results in abnormalities in the physical and structural characteristics of cells. Current research on diseases mainly focuses on the molecular, microbiological, immunological and pathological aspects,

rather than on the mechanical basis, which might make direct contributions to the symptoms and pathophysiological outcomes.

Mechanical processes like pushing, pulling, and squeezing play a remarkably significant role in the biological function of a cell [10-11]. For example, such forces turn out to affect biological processes such as cell growth, division, migration, and death. In addition, mechanical forces at the cellular level impact the function of biological structures ranging from large length scales such as tissues to small length scales such as genes. As a result it is not surprising that when living cells are affected by disease, changes in their mechanical properties also occur. Indeed cell mechanics has been implicated in a variety of diseases, such as cancer [12-14], malaria [15], sickle cell anemia [16], asthma, and glaucoma [17]. For example, Cross *et al.* [12] studied individual cells taken from the tissues of suspected patients with various cancers. From physiology it is suggested that metastatic cancer cells must be more deformable than healthy cells, to be able to invade tissue. Consistent with this notion, individual metastatic cancer cells were indeed found to have lower Young's moduli measured via atomic force microscope (AFM). Also, in suspended state, cancerous and metastatic cells could be distinguished from healthy breast epithelial cells via their resistance to optical stretching [18]. Thus there exists an intimate link between the mechanical properties and the disease state of living cells.

From a mechanics perspective it is well known that intracellular forces are generated and supported via an intracellular framework called the cytoskeleton. This network, containing actin filaments, microtubules, and intermediate filaments, is

dynamic in nature, and is regulated via polymerization and depolymerization rates, which in turn are controlled via molecular motors and ATP [19]. This coupling between intracellular mechanics and chemistry appears to be universal [20-21]. It allows cells to respond mechanically to external stresses by activating biochemical signaling cascades and also underlies the possibility to restore the mechanical properties of diseased cells by pharmacological interventions. Thus cellular mechanotransduction studies that involve understanding and the control of interactions between mechanical forces and biochemical signaling pathways could lead to novel therapeutic strategies to treat diseases.

There are two reasons that characterization of mechanical properties of cells is important. First, studying human diseases from a biomechanics perspective can lead to a better understanding of the pathophysiology and pathogenesis of a variety of human diseases because changes occurring at the molecular and cellular levels will affect, and can be correlated to, changes occurring at the macroscopic level [15]. This will provide an alternative and better approach to assess the onset or progression of diseases as well as to identify targets for therapeutic interventions. Second, cell deformability can serve as a useful biomarker to identify cells depending on disease state, and thus have the potential to be used in human disease diagnostic applications. For example, currently, cancer is diagnosed using a combination of radiological, surgical, and pathologic assessments of tissue samples requiring a microscopic evaluation for diagnosis and prognostic result generation [22]. The methods require significant sample preparation using bench top protocols. The whole process is time consuming and costly. In this

case, cell deformability measurement system can be used as a potential pre-diagnostic tool which can help making a decision for further diagnosis by providing estimation about the disease state in simple and easy way.

1.3 Measuring the Mechanical Properties of Single Cells

Advances in biomechanical tools have led to the wide availability of instrumentations to probe biological cells in physiologically appropriate *in vitro* environments [14]. They have provided new capabilities to generate force vs. displacement records of mechanical deformation for cells. Wide variety of experimental techniques have been developed such as micropipette aspiration, atomic force microscopy (AFM), magnetic twisting cytometry, laser/optical tweezer, microplate stretcher, micro-postarray deformation, and shear flow experiment [14]. In this section, we will take a look at the two most widely used techniques for measuring mechanical properties of cells, the micropipette aspiration and AFM techniques.

1.3.1 Conventional Micropipette Aspiration

Micropipette aspiration is one of the most widely used techniques for measuring mechanical properties of single cells [1]. It is simple and inexpensive but can measure the mechanical properties of cells with a sensitivity and range that is unmatched by any other instrument. Mitchison and Swann [23] first developed the micropipette aspiration method to measure the elastic properties of sea urchin eggs. This method was later used to measure the mechanical properties of red blood cell membranes [24]. This technique

was further developed as a tool to study the viscoelastic properties of membranes and thin-shelled vesicles [25]. Subsequently, it has been employed to study the mechanical behavior of leukocytes [26], blood cells [27], and various other cell types. For example, using the micropipette aspiration technique, Byfield *et al*. have shown that cholesterol depletion increases membrane stiffness of aortic endothelial cells [28], and Hochmuth obtained the Young's modulus of chondrocytes and endothelial cells [1].

Micropipette can be created from a glass tube with an internal diameter of several millimeters. One end of the tube is heated and quickly pulled to a tip with an opening of only a few microns or less. A micromanipulator is used to carefully position a micropipette in contact with a single cell. Figure 1.1 shows the schematic of micropipette aspiration. A known negative pressure (-*P*) is applied, and the cell is partially aspirated into the micropipette. The rigidity of the cell influences the aspiration length (L_p) and outer radius of the cell. These observations can then be used to determine the cellular mechanical parameters (e.g., modulus and viscosity).

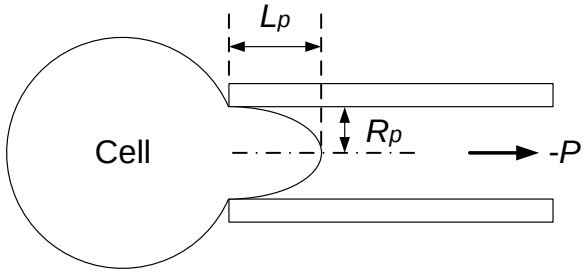

Figure 1.1 Schematic of micropipette aspiration. L_p is the aspiration length of the cell when suction pressure $-P$ is applied to the micropipette. R_p is the radius of the micropipette.

A typical micropipette aspiration system is shown in Figure 1.2. Raising or lowering the reservoir shown in the figure with a micrometer produces a hydrostatic pressure that is greater or less than the pressure in the chamber at the tip of the pipette. A sensitive pressure transducer is connected to the reservoir and calibrated by raising or lowering the reservoir.

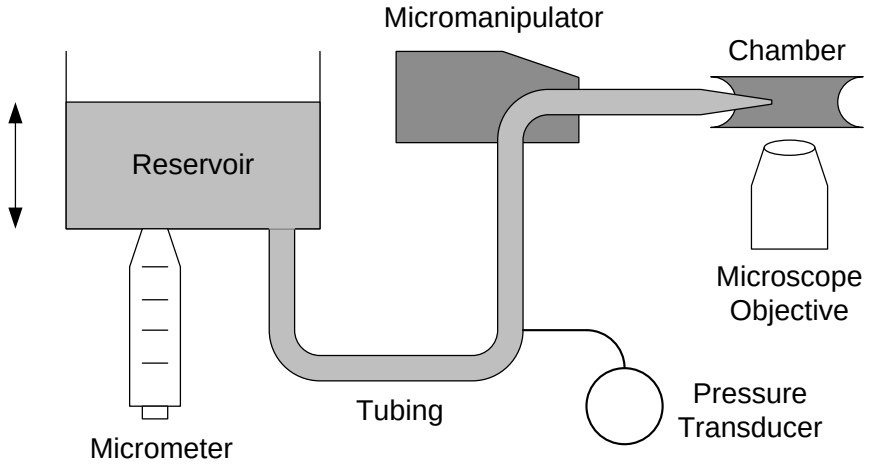

Figure 1.2 Schematic of a micropipette aspiration system.

According to a previously reported researches using micropipette aspiration, biological cells can be classified into two categories, cells that behave as liquid and cells that behave as solid [1].

Neutrophil is an example of liquid-like cells. Micropipette suction is unique in which it can clearly and dramatically show if a cell behaves as a liquid drop with constant cortical tension [1]. This comes directly from the law of Laplace when applied

to the suction of a cell into a micropipette until $L_p/R_p = 1$, the point where the cell forms a hemispherical projection into the pipette. In this case,

$$\Delta P = 2T_c \left(\frac{1}{R_p} - \frac{1}{R_c} \right) \quad (1)$$

where T_c is the cortical tension, R_c is the radius of the cell outside the pipette and P_c is the critical pressure when $L_p/R_p = 1$. Because of the small suction pressures relative to the osmotic pressure of isotonic saline, the cell will deform at constant volume. A further increase in the suction pressure beyond the critical value will cause the radius of the cell outside the pipette to decrease and its reciprocal to increase. It will be impossible to satisfy equation (1) for a cell at equilibrium and, therefore, the cell will flow into the pipette [29].

When cells that behave as solids are aspirated into a micropipette, they do not flow into the pipette when the aspiration length L_p exceeds the pipette radius R_p. The aspiration length increases linearly with the suction pressure regardless of the value of L_p as shown by the experimental data for chondrocytes [30] and endothelial cells [31]. Jones *et al.* further showed that chondrocytes continue to behave as an elastic solid for values of L_p/R_p that are significantly greater than one [30]. According to Theret et al.'s model [31] for micropipette aspiration, when the pipette radius is very small compared to the local radius of the cell surface, the cell can be approximated as an incompressible

elastic half-space. The projection length is predicted to be proportional to the aspiration pressure ΔP and inversely proportional to the elastic modulus as

$$E = \frac{3R_p \Delta p}{2\pi L_p} \phi \tag{2}$$

where E is the Young's modulus, L_p the aspiration length, and R_p is the pipette radius. $\phi(\eta)$ called "wall function", a function of the ratio of the pipette wall thickness to the pipette radius (wall parameter, η) can be obtained using Equation (3) (ϕ = 2.0 - 2.1 when the ratio is equal to 0.2 - 1.0). R_o is the outer radius of the micropipette. Equation (2) will be used to calculate the Young's modulus of HeLa cells to demonstrate the performance of the micro-aspirator chip in Chapter III.

$$\phi(\eta) \approx \frac{1}{2} \cdot \frac{1+\eta}{1+\frac{\eta}{2}} \ln\left(\frac{8}{\eta}\right), \qquad \left(\eta = \frac{R_o - R_p}{R_p}\right) \tag{3}$$

There are two assumptions for this analysis model. First, in order to simplify the model, cells are considered as homogeneous incompressible elastic material. A homogeneous, incompressible material is defined as one which has constant density throughout. Elasticity is the physical property of a material that returns to its original shape after stress (e.g. external forces) - that makes it deform - is removed. In Theret *et al.*'s work, it was assumed that the distribution of organelles and cytoskeletal elements is relatively uniform throughout the cell volume and that the homogeneity of a shear

stressed cell may be analogous to that of a sponge-like material. Second, cell surface was considered as a half-space compared with the size of the micropipette. The ideal case for this model is elongated flattened cells, i.e., cells that do not become spherical after being detached. If these cells are grown on microcarrier beads, micropipette aspiration can be used to obtain the ideal stress-strain relationship of the cell in the attached state.

As we already discussed, micropipette aspiration is a simple, inexpensive, powerful, and versatile method that can provide valuable information about the mechanical properties of cells. However, this technique is currently limited by two major drawbacks. First, micromanipulation of glass micropipettes requires expertise and extensive operating skills. This means micropipette aspiration is a technique for a few trained personnel even though it is a simple and low-cost system. Second, the serial manipulation process severely limits the throughput. These factors prevent the collection of statistically significant quantities of data on a population of cells.

1.3.2 Atomic Force Microscopy (AFM)

AFM is another commonly used technique to determine the mechanical response of individual cells to mechanical forces. Since its invention in 1986 [32], AFM has become one of the most widely used biophysical tools in cell biology because of its ability to image biomolecules at nanometer-scale resolution, apply forces to cells over an extremely wide dynamic range ($10\sim10^6$ pN), and process samples in physiologic media and aqueous buffers.

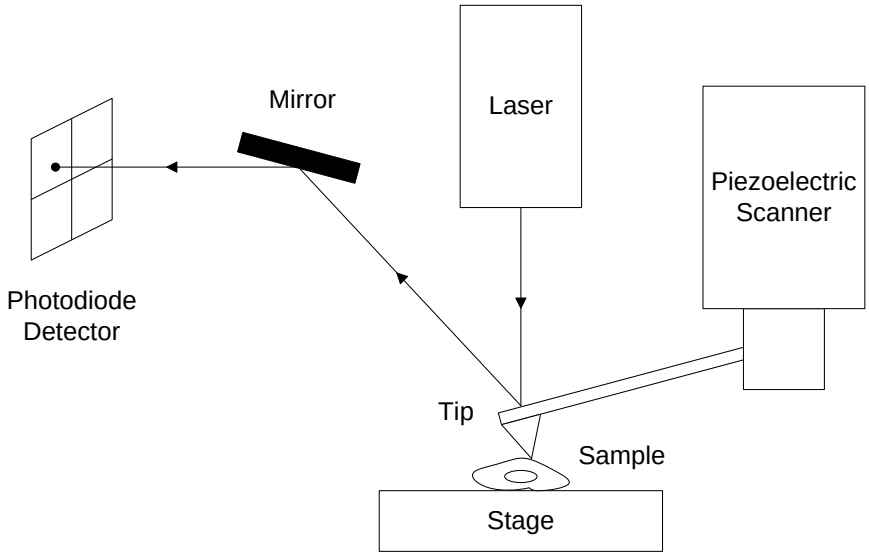

Figure 1.3 Schematic of major components of an AFM.

Major components of an AFM are shown in Figure 1.3. The sharp tip is mounted at the very end of a flexible, microscale cantilever. In a conventional AFM operation mode (usually called contact mode), the tip is brought into close proximity to the sample surface pressing the latter with a small loading force. The tip is next raster scanned over the sample surface, either by moving the sample beneath the tip or by moving the tip over the sample. The movement is controlled by piezoelectric drivers in either a horizontal or vertical dimension. When the tip encounters the sample surface, various forces between the tip and the sample lead to a deflection of the cantilever according to Hook's law. These forces are measured by the amount of deflection of the cantilever. The magnitude of the deflection is captured by a laser beam. The laser beam reflects off

the cantilever, the angular direction of which changes as the tip undergoes deflections. The reflected beams are captured and converted into electrical signals by a position-sensitive photodetector (photodiode). By calculating the difference in signal of the photodiode, the amount of deflection can be correlated with the height, and because the flexible cantilever obeys Hook's law for small displacements, the interaction force between the tip and the sample can be determined. Hence, it is the variation of the point of incidence of the reflected beam on the photodiode that measures any minimal bending or twisting of the cantilever and, thus, the interaction of the tip with the sample. A plot of the laser deflection versus the tip position on the sample surface provides the profile of the hills and valleys that constitute the topography of the surface, and a three-dimensional visualization of the surface topography can be obtained [33].

In cell biology, AFM is mainly used for cell imaging and force detection. AFM imaging has been widely used for studying the structures and mechanics of isolated biomolecules [34-36], components of cell nucleus [37-38], and subcellular cytoskeletal structures [39-40]. In addition to imaging, AFM has been successfully used in a force mode in which the tip is held in a fixed horizontal position and used to indent a sample. This approach has been applied with great success to measure the mechanical properties of many different cell types [41-45] and alterations in stiffnesses associated with cell differentiation [46] and disease progression [47-49]. Using AFM, Cross *et al*. have shown that the cell stiffness of metastatic cancer cells is more than 70% lower than the benign cells [12].

Although this method has significant advantages such as high resolution and accurate location measurement, it suffers from disadvantages such as difficulty in sample finding, onerous cell immobilization steps, and potential damages of the samples due to the direct contact between the tip and the sample. Particularly, immobilization of "cell samples" on substrates is a crucial step [50]. Coupling AFM with microscope technique is one way to solve the difficult sample finding issue. Several cell immobilization methods for AFM have been reported. First, air-dried method which dries cell samples on the substrate is very simple but dehydration during the drying process can affect cell morphology. Bolshakova *et al.* modified glass slides with poly-L-lysine that is positively charged at physiological pH [51]. As cell surfaces are negatively charged at physiological pH, cells could be immobilized on these modified glass slides through electrostatic interaction. This cell immobilization method is simple and reproducible, and is currently the most frequently used method. However, disadvantage of this method is that poly-L-lysine may interact with cells and possibly induce structural alternations. In 2004, Lu's group [52] immobilized living bacterial cells on agarose gel coated surfaces and imaged them with AFM. The agarose layer could immobilize cells firmly and provide the necessary nutrients and a relatively wet environment to prevent cell alteration. So this method is more suitable for keeping the native state of cell than poly-L-lysine method. However, the procedure is relatively complicated.

Although many efforts to overcome the issues of AFM have been made, AFM still have a critical limitation which is its inherent low throughput. Operator need to pic up every starting points of the measurement on the samples by manipulating the AFM

tip. This process is very time consuming and also needs expertise and extensive operator skills. In addition, onerous and complicated cell immobilization step is still required for cell sample measurement. Although it is becoming a common technique, AFM still needs expensive equipment. Due to these reasons, AFM is not suitable for routine quantification of mechanical parameters of biological cells in statistically significant quantities.

1.4 Microfluidic Devices for the Measurement of Mechanical Properties of Single Cells

Microfabrication is a method for constructing systems and structures at micron or submicron scales first developed for semiconductor devices. Its scale of size is well matched to the physical dimensions of biological cells [2], and microfluidic - the manipulation of fluids in channels with dimensions of tens of micrometers - devices make it possible to manipulate individual cells and their immediate extracellular environments [53]. Soft lithography refers to a collection of techniques for creating microstructures and nanostructures based on printing, molding and embossing [3]. One useful characteristic of soft lithography is that hundreds of replicas of the inverse pattern can be produced in PDMS from one master [2]. PDMS has been the most widely used material for the applications of soft lithography in biology, because of the following characteristics: it is soft, flexible, biocompatible, insulating, unreactive, transparent to ultraviolet and visible light, permeable to gases and only moderately permeable to water [54-55]. The prepolymer of PDMS is commercially available, inexpensive, and easy to

prepare. Due to these advantages, PDMS microfluidic systems have applications in the extensive study of many areas of cell biology, including the cytoskeleton [56], the forces exerted by cells on the substrate to which they are attached [57], the contents of cells (down to the single-cell level) [58-59] and the stiffness of cells.

Previous studies have shown that microfluidic device can be used to measure the stiffness of biological cells. These studies can be classified into two categories, flow-through type and micropipette aspiration type.

1.4.1 Flow-through Type Microfluidic Devices

Flow-through type microfluidic devices were extensively used to characterize the complex behaviors of single cells by measuring several parameters such as the transit time and shape recovery time for single cells to pass through a narrow channel. The transit times can be recorded using optoelectronic [60] or resistive pulse detection [61] methods. Instead of using a single pore, recently, Rosenbluth *et al.* [62] performed many parallel measurements using a microfluidic binary tree network that consists of successive bifurcations of a large channel into smaller channels. In this study, cell size and transit times were measured using automated image processing methods. This allowed them to delineate the dependence of transit times on cell size and cell deformability and thus establish a link between transit time distributions, cell deformability, and their diseased state. Hou *et al.* has shown that simple microfluidic device can be used to distinguish the difference in stiffness between benign breast epithelial cells (MCF-10A) and non-metastatic tumor breast cells (MCF-7) [4]. In 2003,

Shelby et al. qualitatively showed that late-stage schizonts can cause blockages in narrow elastomeric channels, which were used to mimic the narrow capillaries found in the human body [6]. In 2006, Lee *et al.* designed an on-chip erythrocyte deformability test using microfluidics to distinguish cancerous blood from normal blood [5]. They have defined useful parameters which are linked to the inherent deformability of the cancerous cells and plotted 2D and 3D graphs using these parameters. This proved to be effective as they could discriminate cancerous blood population from normal ones with better sensitivity and reliability. Although flow-through type microfluidic devices can provide valuable information about the mechanical properties of cells, it has the limitation that one device cannot be used for different kinds of cells. Since there is no theoretical model developed such as for micropipette aspiration, parameters have to be defined for each channel design. In addition, depending on the parameters which need to be measured, expensive and bulky equipments may be needed.

1.4.2 Microfluidic Micropipette Devices

Micropipette array chip that can measure the deformation of four L929 fibroblasts simultaneously has been reported by Moraes *et al.* [7]. Although it showed the potential of microfluidic micropipette aspiration device, its design had limitations. Lateral cell trapping and deforming technique was used due to its straightforward working principle, simple channel design and fabrication. Two microfluidic channels of different sizes in plane form a fluidic junction. The main channel is large enough to let cells pass through and the trapping channel is not. Applied pressure through the trapping

channel simply attracts a cell form the main channel and traps it at the junction. This simple mechanism and geometry have strong potentials since they are simply realizable by micro-casting of soft lithography using polydimenthylsiloxane (PDMS) [3]. However, soft lithography has inherent limitations. Since it uses replications of on-plane patterns, the replicated patterns are on the same plane. In the case of microfluidic replication, the whole microfluidic channels share one sidewall and this can cause unnatural deformation of the cells as shown in Figure 1.4 (a). Good seal between the cell and the aspiration channel is essential for micropipette aspiration and nonsymmetrical cell deformation can greatly affect accurate measurement. In addition, this lateral cell trapping method to trap the free-floating cells into the aspiration channel is very time consuming and needs high suction pressure.

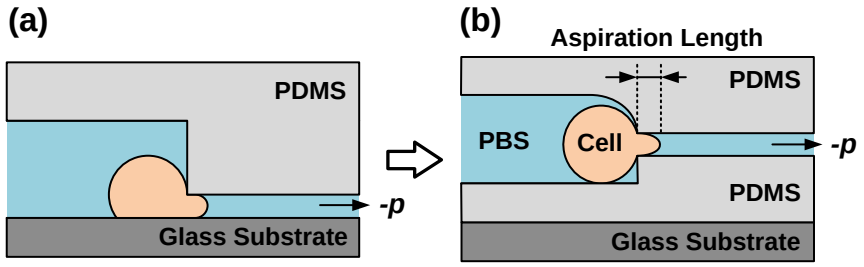

Figure 1.4 (a) Cross-sectional view of a cell undergoing aspiration into a microfluidic channel. (b) Cell aspiration into a raised microfluidic channel.

This issue can be solved by an elevated aspiration channel shown in Figure 1.4 (b). This design allow symmetric cell trapping at the self-raised junction, so that aspiration pressure distributes uniformly on cellular membranes. Lee's group has reported several methods to avoid unnatural deformation of the cell for patch clamp application such as lateral cell trapping sites raised above the bottom plane of the chip [63] and self-raised circular orifice using vacuum expansion [64] but such raised structure has not been used in microfluidic micropipette applications.

CHAPTER II

DEVELOPMENT OF THE MICRO-ASPIRATOR CHIP

2.1 Design Principle

As we discussed in Chapter I, traditional glass micropipette aspiration and AFM suffer from their inherent low throughput and recently developed microfluidic micropipette devices have limitations such as difficult cell trapping and unnatural cell deformation. In order to address these limitations, we propose a high-throughput micro-aspirator chip, which can deliver, trap, and deform multiple cells simultaneously with single-cell resolution without the need for skill-dependent micromanipulation. The micro-aspirator chip is composed of 40 arrays of cell traps and aspiration channels that can apply suction pressure to a trapped cell. In this section, design principle of cell trapping and deformation will be described and the dimension of the actual device will be shown.

2.1.1 Hydrodynamic Trapping of Single Cells

In order to measure the mechanical properties of cells using microfluidic micropipette chip, individual cells need to be trapped at the entrance of an aspiration channel. One of the most robust methods to trap cells in relatively high throughput is using microwell arrays [65-67]. These platforms allow thousands of single cells to be randomly captured by gravity at the bottom of a microwell. However, this trapping method is not appropriate for micropipette aspiration applications since a single empty

trap will vary the applied pressures at every other well. On the other hand, microfluidic valves, optical tweezers, dielectrophoresis (DEP), and acoustic waves are powerful approaches to trap and manipulate single cells [68]. However optical tweezers or valve-controlled devices typically are able to handle only one or a few single cells at once, and although DEP-based systems have a higher throughput, they are less suitable for maintaining cell conditions during the measurement due to high temperature induced by Joule-heating.

A family of emerging technologies that combines active single cell handling with the potential for high-throughput experimentation is microfluidic hydrodynamic traps. Cells are drawn into the trap by flow that can either be generated using pressure [69-70], pump driven control channels [71-72], or by re-connecting the gap to the main channel [73-75]. In the latter case, one fraction of the flow crosses the trap and the other fraction passes through the main channel [76]. Once the trap is filled, the flow through the trap is reduced and thus no additional cells can be trapped [73]. An example of such a 'self-regulating' trap device has been presented by Tan *et al.* [77]. Using polymer beads, these authors demonstrated that the efficiency of hydrodynamic single bead trapping depends on the ratio of the flow through the trap and the main channel. Furthermore, they correlated this ratio with the fluidic resistance of the trap and the main channel, and obtained a perfect bead trapping efficiency of 100% with a ratio of 1 : 3 [77]. Recently, Kobel *et al.* optimized the microchannel dimension and flow rate for single cell trapping using the same scheme [78].

A micro-aspirator chip was designed based on the cell trapping method first reported by Tan *et al*. [77]. Figure 2.1 (a) shows the schematic of the microfluidic trap.

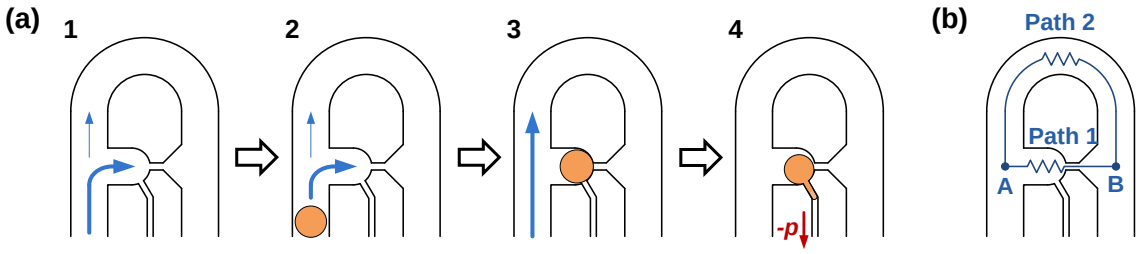

Figure 2.1 Schematic diagram of the cell trapping and cell aspiration principle. (a) (1, 2) When the trap is empty, flow resistance along the straight channel is lower than that of the loop channel, and the main flow stream goes through the cell trap. (3) Once a cell is trapped, the main flow stream goes through the loop channel. (4) Negative pressure is then applied to aspirate the trapped cell. (b) Schematic of flow resistance.

It is composed of serpentine channels superimposed onto a straight channel, with narrowed regions along the straight channel functioning as traps. The channels are designed such that when a trap is empty, the straight channel has a lower flow resistance than that of the loop channel. As a result, bulk of the fluid flows through the straight channel. A cell in the flow will be carried by this main stream into the trap (trapping mode). This cell acts as a plug, increasing the flow resistance drastically through the straight channel, and redirecting the main flow to the loop channel. Subsequent cells will then be carried along the loop channel, by passing the filled trap (bypassing mode). Using series of this trap, a cell trapping array can be realized where cells are trapped in

sequence from the very first trap. Using the Darcy-Weisbach equation, pressure difference between two points inside a microchannel can be calculated as

$$\Delta p = \frac{C(\alpha)}{32} \cdot \frac{\mu L Q P^2}{A^3} \tag{4}$$

where $C(\alpha) = f \times Re$ (f: Darcy friction factor, Re: Reynolds number), μ is the fluid viscosity, L is the length of the channel, Q is the volumetric flow rate, P is the perimeter for the channel and A is the cross-sectional area of the channel. In Figure 2.1 (b), fluid can flow from junction A and B via path 1 and 2. Equation (4) can be applied separately for paths 1 and 2, and because the pressure drop is same for both paths, we can calculate the flow rate of path 1 (Q_1) and 2 (Q_2). If Q_1 is greater than Q_2, the cell will be captured inside the trap.

Before the fabrication of the cell trapping device, we tested several microfluidic channel designs that can trap 90 μm diameter microbead. Three different ratios of the fluxes through the trap (Q_1) and the main channel (Q_2), 1.5:1, 2:1 and 3:1 were tested and successful bead trapping with almost 100% efficiency was observed in all three cases. Microbead suspension was injected into the inlet of the microchannel by pushing the syringe manually. Figure 2.2 shows microscopic images of the microbeads trapped in order when the flux ratio was 3:1.

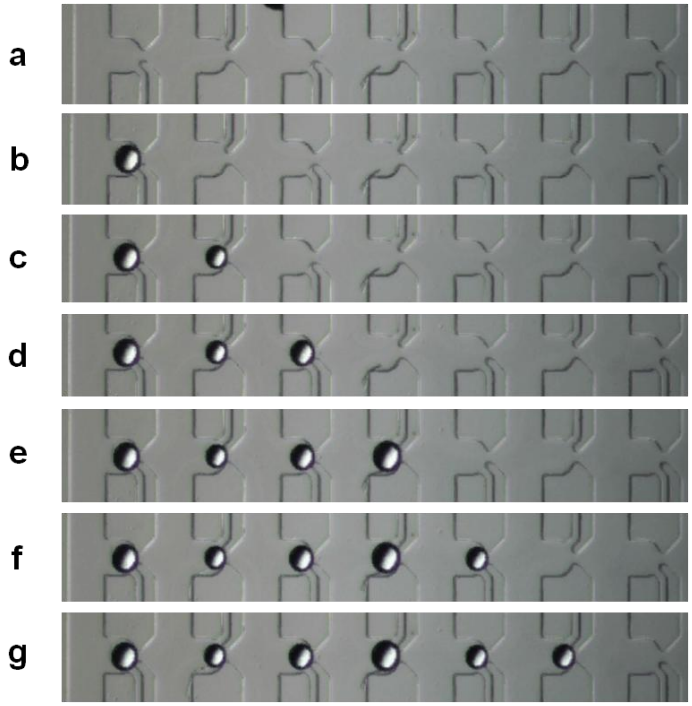

Figure 2.2 Microscopic images of microbead trapping when the ratio of the fluxes through the trap (Q_1) and the main channel (Q_2) was 3:1. The beads (90 μm diameter) were trapped in sequence from the very first trap.

Based on this result, a flux ratio 3:1 was used to design the real micro-aspirator chip for cell trapping. Figure 2.3 shows the overall design and dimension of the micro-aspirator chip. It consisted of 40 cell traps, and all traps were connected to aspiration channels through which suction pressure can be applied. The width of the cell trap and the aspiration channel is 15 μm and 3 μm respectively.

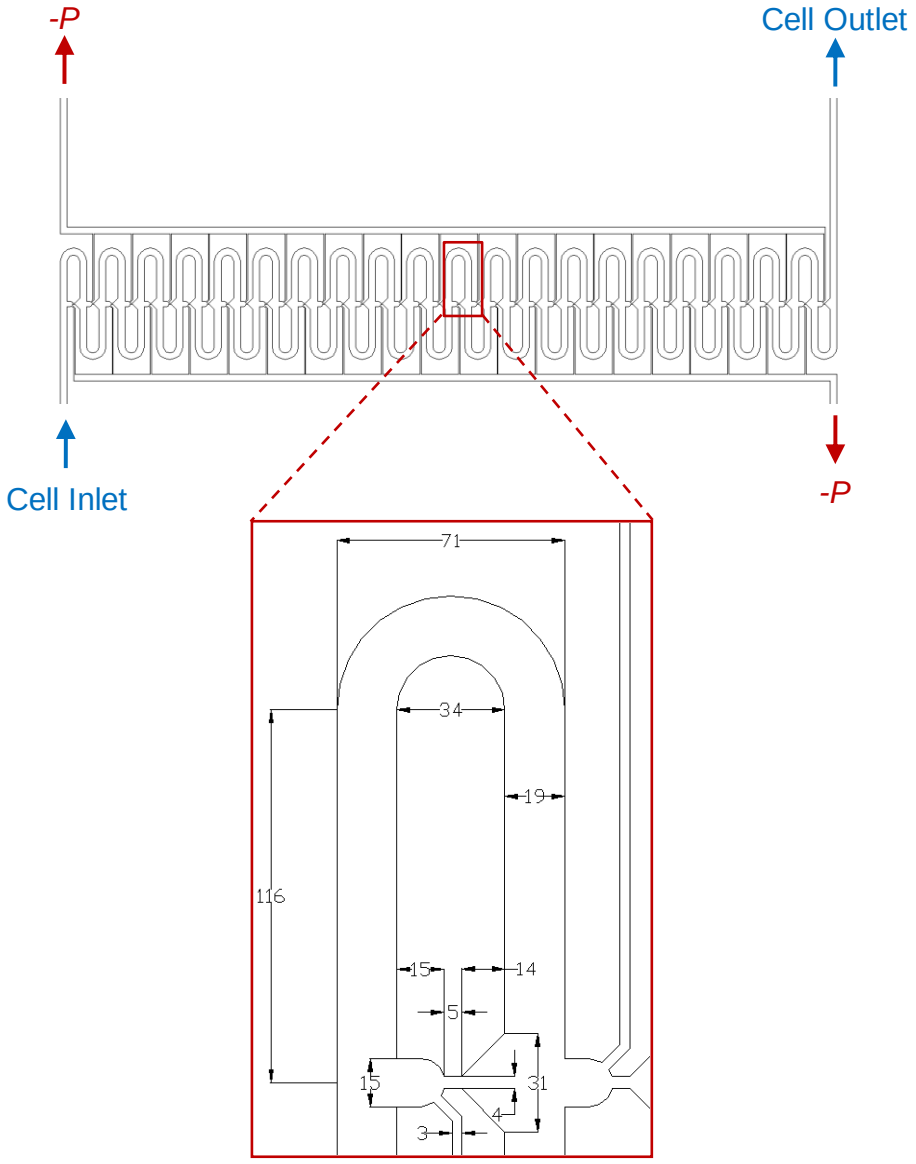

Figure 2.3 Overall design and dimensions of the micro-aspirator chip (unit: μm)

2.1.2 Deforming Single Cells

As shown in Figure 1.1 (a), recently developed microfluidic micropipette device has unnatural cell deformation issue. This issue could be solved by positioning the

aspiration channel at the center of the cell both in vertical and horizontal direction as shown in Figure 1.1 (b).

After all traps are filled with cells, negative pressure can be applied to the aspiration channel using hydrostatic pressure. The reservoir setup that was used to deform the cells through the aspiration channel was based on the working principles of a manometer. Briefly, the pressure generator setup involved the use of two reservoirs held at the same level with a retort stand. The reservoirs were filled with phosphate buffer solution (PBS) where the pressure generated in the microfluidic channels is governed by a simple mathematical equation:

$$\Delta P = \rho g h \tag{5}$$

where ΔP is the pressure difference between the reservoir, h is the height difference of PBS between the reservoir, ρ is the density of 1×PBS, and g is the gravitational acceleration. In the hydrostatic pressure generation system for micro-aspirator chip, the outlet of the microfluidic channel can be considered as one reservoir and the tube filled with PBS can be considered as the other. A pressure transducer was used to accurately measure the amount of pressure applied. We could observe that the measured value of pressure using the transducer and the height difference followed the linear relation in equation (5).

2.2 Microfabrication

The micro-aspirator chip was fabricated using photolithography, soft lithography and PDMS membrane vacuum expansion method. Figure 2.4 shows the schematic of the microfabrication process.

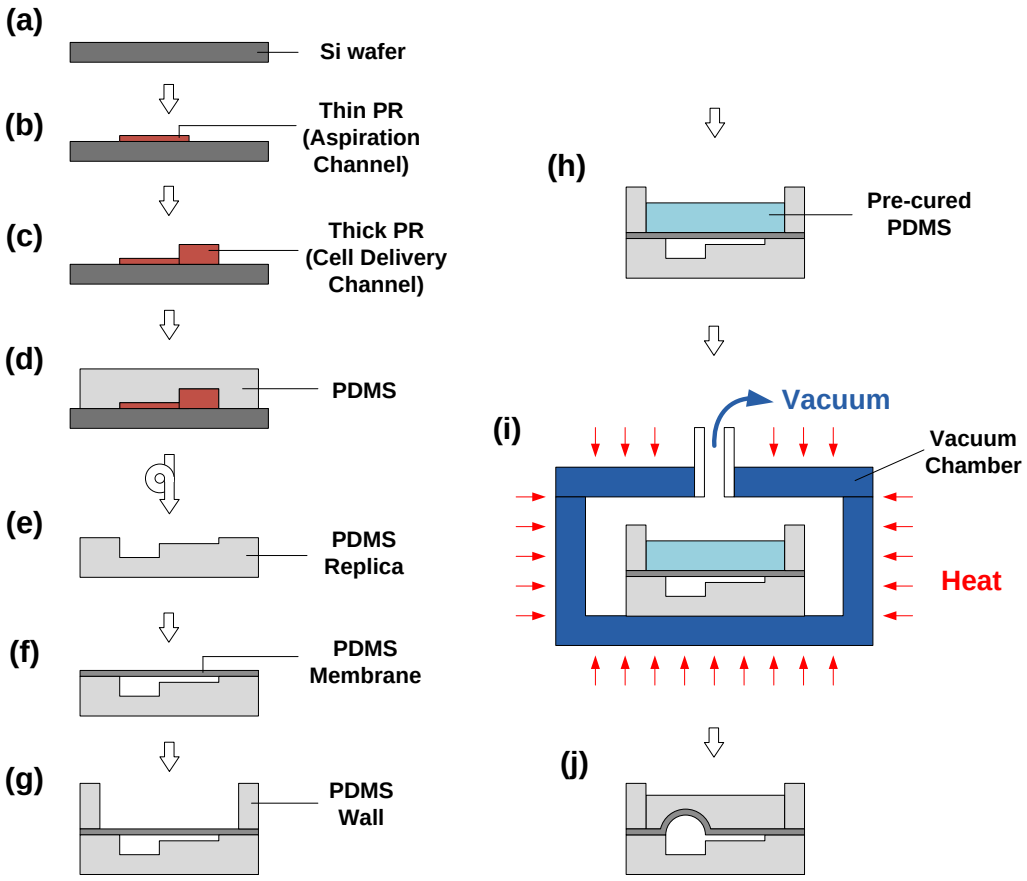

Figure 2.4 Schematic of the microfabrication steps. (a) Bare silicon wafer. (b) Aspiration channel patterned silicon wafer using SU-8™ 2002. (c) Cell delivery channel patterned silicon wafer using SU-8 ™ 2007. (d, e) PDMS replication process. (f) PDMS membrane attached to the PDMS replica. (g) PDMS wall structure attached. (h) Pre-cured PDMS poured inside the wall structure. (i) Whole device placed inside a vacuum chamber. Vacuum and heat were applied at the same time. (j) Vacuum expanded microfluidic channels resulting in raised cell aspiration channel.

Briefly, the 3 μm-thick cell aspiration channels were patterned on a silicon wafer via a lithography process with SU-8™ 2002 (Figure 2.4 (b)). After development, 9 μm-thick cell delivery channels were patterned using SU-8™ 2007 (Figure 2.4 (c)). A PDMS layer was replicated from the SU-8™ mold (Figure 2.4 (d, e)). In order to make the 3 μm-thick PDMS membrane, PDMS and hexane mixture (PDMS : hexane = 1 : 3 (w/w)) was spin-coated at 4500 rpm for 30 seconds on a trichlorosilane coated silicon wafer and cured inside an oven for 15 min. After oxygen plasma treatment, the PDMS membrane was bonded to the PDMS replica (Figure 2.4 (f)). After attaching the wall structure made with PDMS, PDMS pre-mixture was poured on the membrane. Once the whole device was placed inside a vacuum chamber, vacuum (1.3 Pa) and heat (130°C) was applied simultaneously for 12 min. Pressure difference between inside and outside of the enclosed microfluidic channel caused expansion of the membrane, mainly on the cell trap and the cell delivery channel. Due to the narrow width of the aspiration channel (3 μm), however, the membrane on the aspiration channel was not expanded.

2.2.1 Photolithography to Form the Soft Lithography Master Mold

The master mold was fabricated on a 3 inch diameter silicon substrate using a two-layer photolithography process by sequentially patterning two layers of photosensitive epoxy (SU-8™, Microchem, Inc., Newton, MA) with different thicknesses. The first layer forming the aspiration channels was 3 μm thick and the second layer forming the cell delivery channels and cell traps was 9 μm thick.

First, aluminum alignment marks were patterned on a silicon wafer through a lift-off process. These alignment marks are used to align the aspiration channels and the cell delivery channels that will be patterned separately. Microposit S1818 photoresist (Rohm and Haas Electronic Material LLC, Marlborough, MA) was spin coated on bare silicon wafer at 4000 rpm for 30 seconds with an acceleration time of 10 seconds. Next, the substrate was soft baked at 100°C for 10 minutes. The substrate was then exposed using a mask aligner (MJB3, SUSS MicroTec Inc., Waterbury Center, VT) at 12 mW/cm^2 (wavelength: 320 nm) for 14 second with a photomask having alignment marks. After baking at 130°C for 10 minutes, the substrate was developed (MF-319, Rohm and Haas Electronic Material LLC, Marlborough, MA) for 20-40 seconds. The substrate was then rinsed in DI water and dried with N_2 gas. The resulting silicon wafer was covered with photoresist with only the alignment marks opened. An aluminum layer was evaporated on the substrate using an E-beam evaporator to a thickness of 2500 Å. In order to remove the sacrificial photoresist layer, the substrate was sonicated in aceton, isopropyl alcohol (IPA) and DI water for 10 minutes, respectively.

In order to pattern the aspiration channels, 3 μm thick photoresist (SU-8™ 2002, Microchem, Inc., Newton, MA) was spin-coated on the alignment mark pattered silicon wafer at 750 RPM for 30 seconds, followed by baking on a 95°C hotplate for 4 minutes. The substrate was then exposed using a mask aligner (MA6, SUSS MicroTec Inc., Waterbury Center, VT) at 200 mJ/cm^2 with a photomask having aspiration channel patterns. After exposure, the substrate was baked at 95°C for 4 minutes, and then

developed (Microposit Thinner Type P, Shipley Co., Marlborough, MA) for 1 minute. Finally, the substrates were rinsed in DI water and dried with N_2 gas.

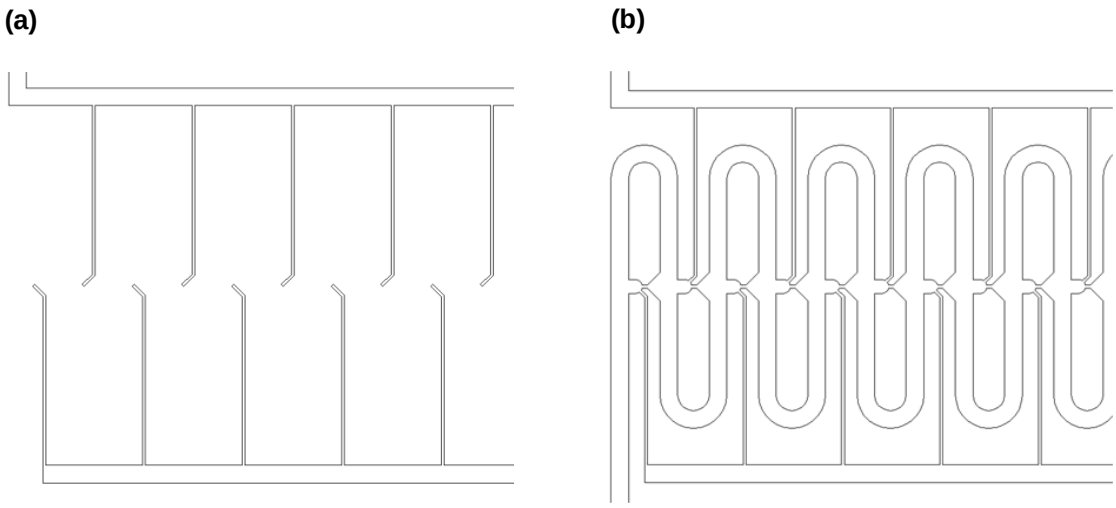

Figure 2.5 2-D schematic of the two layer photolithography. (a) 3 μm-thick cell aspiration channel patterned using SU-8™ 2002 photoresist. (b) 9 um-thick cell delivery channel patterned on top of the aspiration channel patterns using SU-8™ 2007. The end of the aspiration channels meets the cell trapping sites.

Photoresist (SU-8™ 2007, Microchem, Inc., Newton, MA) for patterning the cell delivery channel (9 μm-thick) was spin-coated on the silicon wafer at 2500 rpm for 25 seconds with an acceleration time of 5 seconds, followed by baking at 95°C for 5 minutes. The substrate was then aligned and exposed using a mask aligner (MA6, SUSS MicroTec Inc., Waterbury Center, VT) at 180 mJ/cm^2 with a photomask having cell delivery channel patterns. The substrate was baked at 95°C for 5 minutes, and then

developed (Microposit Thinner Type P, Shipley Co., Marlborough, MA) for 1 min. As a final step, the substrates were rinsed in DI water and dried with N_2 gas.

2.2.2 Photoresist Reflow

Microchannels with semicircular cross section can be fabricated through vacuum expansion of a PDMS membrane which will be explained in the following section. This means if we can make a semicircular microchannel master mold, PDMS channel having a round-shaped cross section can be fabricated. Round-shaped aspiration channel is advantageous in micropipette aspiration applications since good seal between the cell and the aspiration channel can be achieved and existing analytical models can be used to interpret the results. In order to make rectangular cross section of microchannels of a master mold to semicircular, photoresist reflow method was tried using SU-8™ and Futurrex patterns.

First, SU-8™ 2002 (Microchem, Inc., Newton, MA) microchannels were patterned on a silicon wafer using conventional photolithography techniques and three different reflow conditions, 12 hours at 220℃, 10 hours at 250℃ and 1 hour at 285℃. Reflowed SU-8 pattern were sputter coated with 100Å of Au in argon plasma. Images were acquired using a scanning electron microscope (SEM) (12 kV acceleration, JEOL 6400, JEOL Ltd., Tokyo, Japan). Figure 2.6 shows the SEM images of reflowed SU-8™ patterns. Although the edge of the channels became slightly smoother, the overall cross section did not changed significantly from its original rectangular shape.

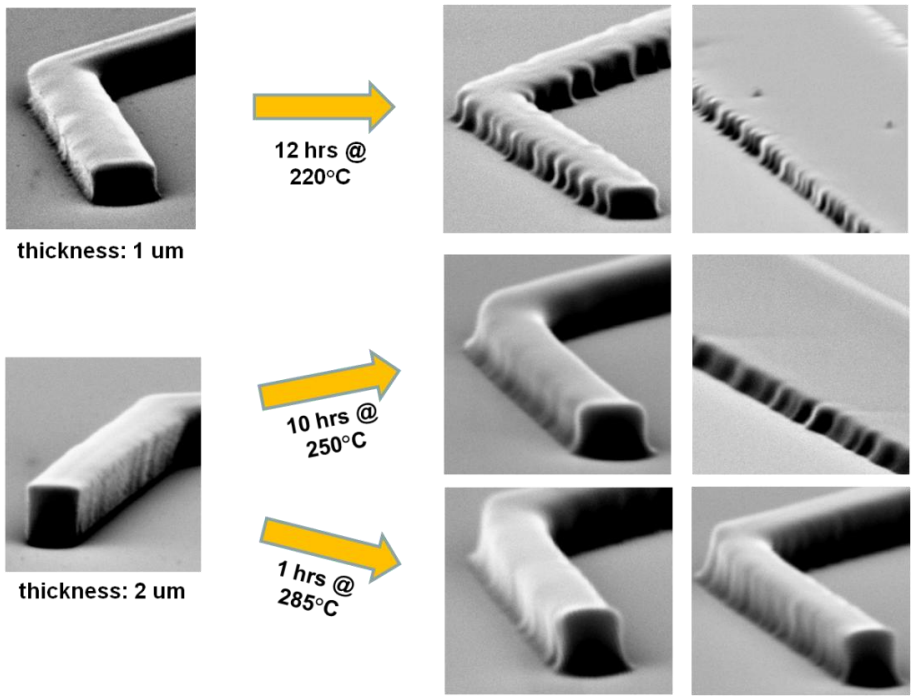

Figure 2.6 SEM images of reflowed SU-8™ ridge structure.

Futurrex (NR4-8000P, Futurrex, Inc., Franklin, NJ) patterns were heated on a 150℃ hotplate for 15 minutes and 1 hour. As shown in Figure 2.7, after the photoresist is reflowed, the cross section of the channels changed to a circular shape. There was almost no difference of the curvature between 15 minutes and 1 hour of reflow. Profile of the reflowed channel was analyzed using an optical microscope (Eclipse LV100, Nikon Instruments Inc., Melville, NY), optical surface profilometer (Veeco NT9100, Veeco, Plainview, NY) and stylus profiler (Dektak3, Veeco Instruments Inc., Plainview, NY). Although the reflow was successful, all aspiration channels were removed during the development process of the cell delivery channels and this method couldn't be used for the fabrication of the micro-aspirator chip.

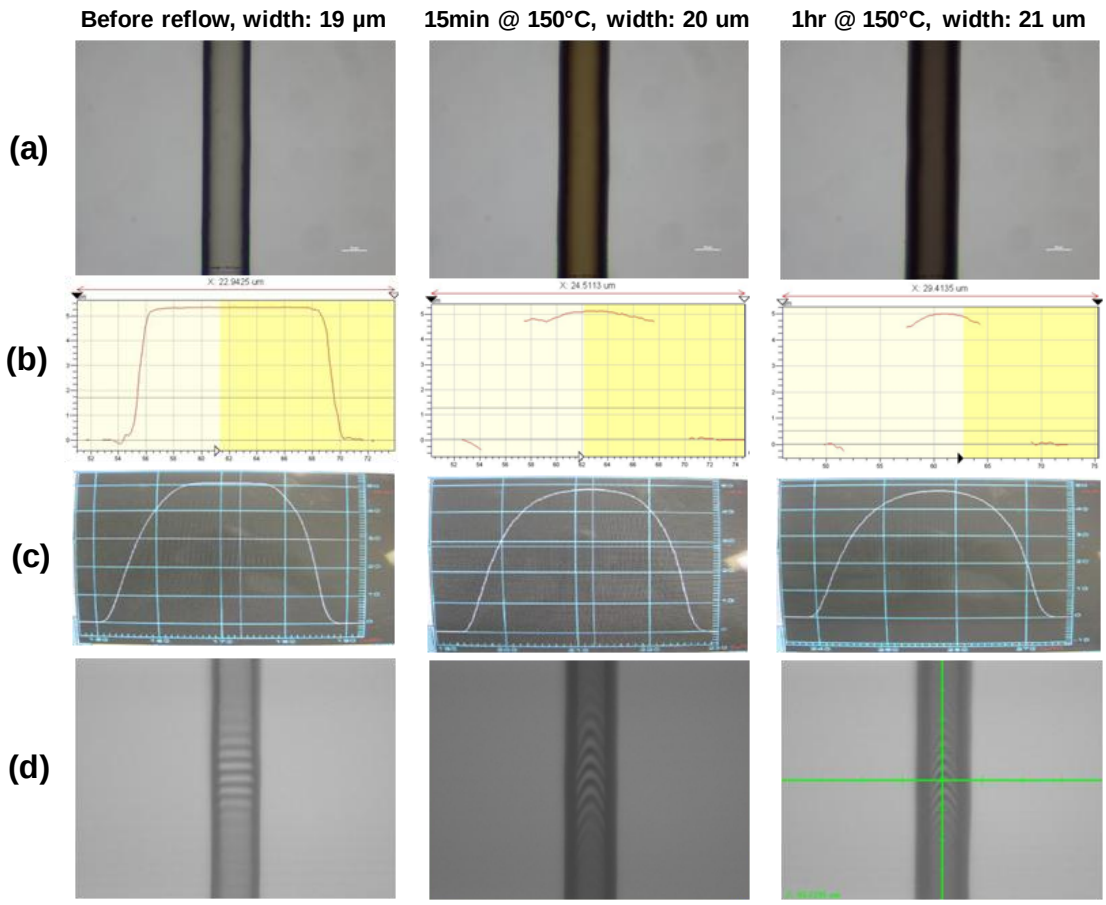

Figure 2.7 Reflowed Futurrex NR4-8000P. (a) Images taken using upright Nikon microscope. (b) Profile measured by Veeco optical profilometer. (c) Profile measured by Dektek. (d) Fringe images using Veeco optical profilometer.

2.2.3 Replication of the Master Mold Using Soft Lithography

The SU-8™ master that has the aspiration channel and the cell delivery channel patterns was coated with (tridecafluoro-1,1,2,2-tetrahydrooctyl) trichlorosilane (United Chemical Technologies, Inc., Bristol, PA) inside a desiccator for 15 min to facilitate PDMS release from the master after replication. PDMS layer was replicated from the master by pouring PDMS pre-polymer (10:1 mixture, Sylgard® 184, Dow Corning, Inc.,

Midland, MI), followed by curing at 85°C for 40 min. This process resulted in partial success where small SU-8™ patterns such as the aspiration channels were peeled off or partially damaged after repeated replication. This issue could be solved by using a polyurethane master instead of SU-8™ mold, a method first developed by Desai *et al.* [79]. Figure 2.8 shows the polyurethane master fabrication and PDMS casting processes.

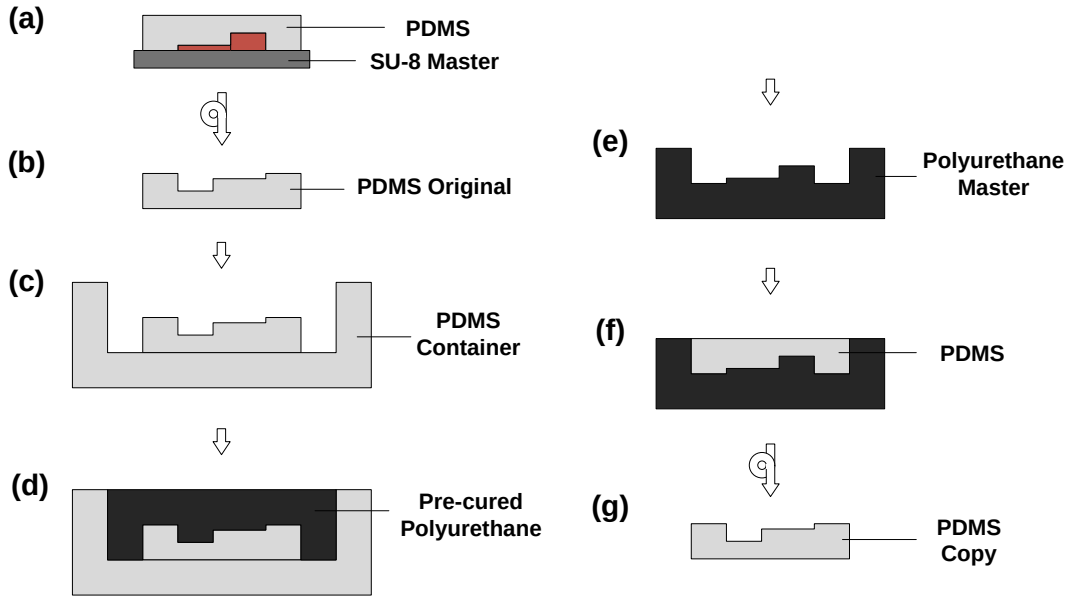

Figure 2.8 Polyurethane master fabrication and PDMS casting steps. (a, b) PDMS original was replicated from the SU-8™ master. (c) PDMS original was bonded on the bottom of a PDMS container. (d) Pre-cured polyurethane mixture was poured into the PDMS container. (e) After the polyurethane was fully cured, it was removed from the container. (f) Pre-cured PDMS mixture was poured into the polyurethane master. (g) After curing, PDMS copy can be fabricated which has same pattern as the PDMS original.

Polyurethane masters were fabricated using a commercially available two-part polyurethane plastic (Smooth Cast 310, Smooth-On Inc., Easton, PA). The PDMS original to be molded was first affixed to the bottom of an open-topped container constructed of PDMS (Sylgard® 184, Dow Corning, Inc., Midland, MI). Since the polyurethane plastic does not adhere to silicone surfaces, the open-topped PDMS container ensures that the plastic precursor is only in contact with silicone surfaces. The PDMS container provided a reusable means for casting the polyurethane masters and obviated the need for any surface treatments in the casting process. A thin seed layer of PDMS (mixed in a 10 : 1 ratio and subsequently degassed) was poured in the bottom of the container and the device was placed on top of it, after which the container and device were placed in a 85°C convection oven for 1 hour to cure and hence bond the device to the container. In the meantime, the two parts of the plastic pre-cursor (parts A and B) were measured out in equal volumes and degassed separately for approximately 10 min. Parts A and B were then mixed together slowly taking care to avoid bubbles and liquid plastic pre-cursor mixture was poured into the container. The plastic was then left to cure on a level surface for 2 hours at room temperature. Upon curing, the polyurethane master was removed from the container and ready for molding with PDMS. PDMS devices were fabricated from polyurethane master using conventional soft lithography molding techniques. Briefly, PDMS was mixed in a 10 : 1 base : hardener ratio and subsequently degassed in a vacuum chamber for 30 minutes. Degassed PDMS was then poured directly on the polyurethane master and then left to cure at 85°C for 1 hour.

2.2.4 Vacuum Expansion

Vacuum expansion method first reported by Seo *et al.* [64] was used to make the semicircular cell delivery channels and the cell traps. The vacuum expansion process took 12 minutes through process optimization, significantly reducing the previously reported 24-hour processing time [64]. Figure 2.9 shows the 3-D schematics of the vacuum expansion process.

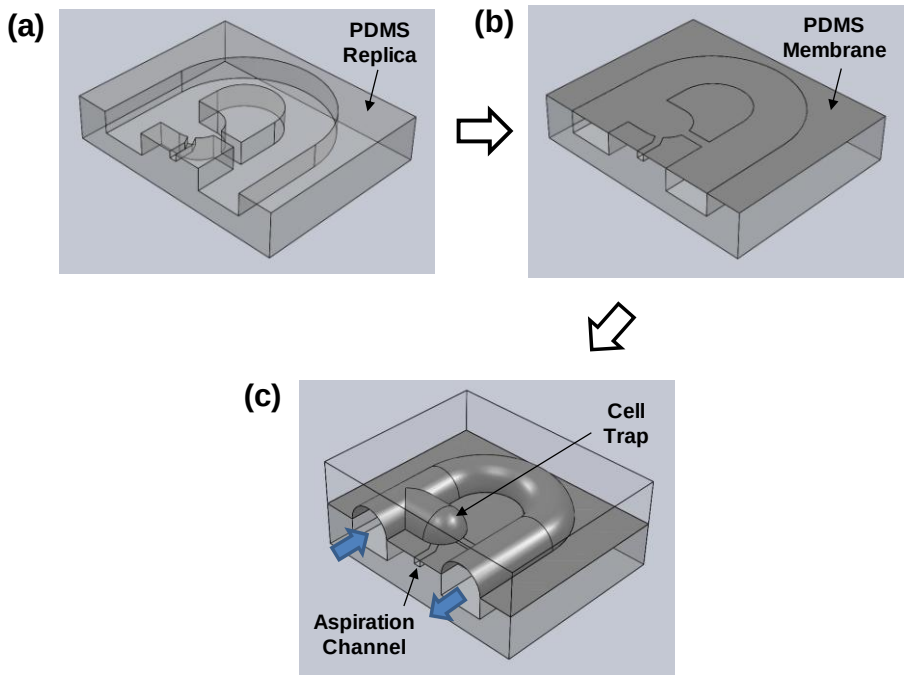

Figure 2.9 3-D schematic of the vacuum expansion steps. (a) PDMS block made out of a double-layer SU-8™ master. (b) PDMS membrane bonded on the microfluidic layer. (c) Vacuum expanded microfluidic channels.

In order to optimize the PDMS membrane thickness for vacuum expansion, several different thicknesses and channel sizes were tested. Three different mixing ratio

of PDMS and hexane (PDMS : hexane = 1 : 1, 1 : 3 and 1 : 5 (w/w)) were spin-coated at 4500 rpm for 30 sec on a trichlorosilane coated silicon wafer and cured inside the oven for 15 min. Cross section of the device was observed using an optical microscope (Eclipse LV100, Nikon Instruments Inc., Melville, NY). Membranes having thickness of 7 µm, 2 µm and 1 µm were obtained using mixing ratios of 1 : 1, 1 : 3 and 1 : 5 (w/w) respectively. Figure 2.10 shows the results of the vacuum expansion test using different width of straight channels. 1 and 2 µm-thick membranes attached to 100 µm-wide channel were collapsed and couldn't be expanded. This represents the ratio between the channel geometry (depth and width) and the PDMS membrane thickness needs to be optimized for the vacuum expansion method.

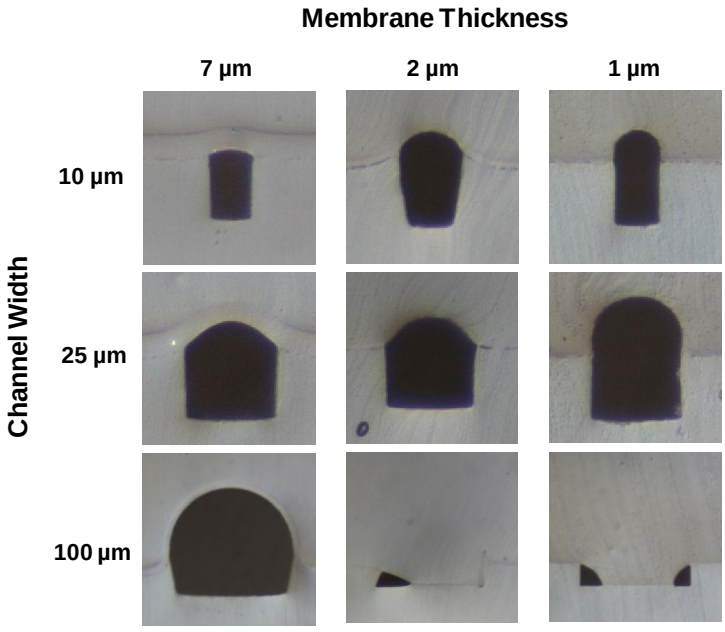

Figure 2.10 Vacuum expansion preliminary test results. 1 and 2 µm-thick membranes attached to 100 µm-wide channel were collapsed and couldn't be expanded.

Figure 2.11 shows the membrane thickness optimization process using the actual micro-aspirator device PDMS layer. When PDMS thickness was 7 μm, expansion was not enough. 1 μm-thick membrane collapsed and attached to the bottom of the channel during the membrane bonding process. Cell delivery channels were sufficiently expanded using a 2 μm-thick membrane.

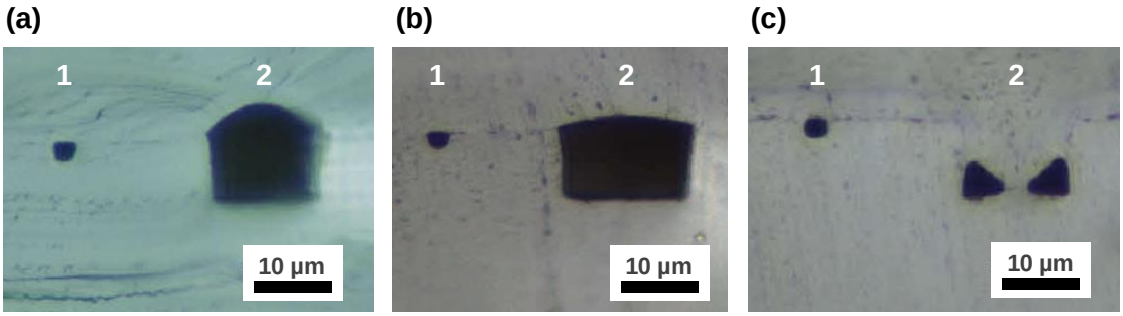

Figure 2.11 Vacuum expansion process optimization. Microscopic images of cross sections of the aspiration channels (1) and the expanded cell delivery channels (2). (a) PDMS membrane thickness: 2 μm, sufficient expansion. (b) PDMS membrane thickness: 7 μm, insufficient expansion. (c) PDMS membrane thickness: 1 μm, collapsed membrane attached to the bottom of the channel.

The vacuum expansion process is as following. The pre-mixture of PDMS was cross-linked on a polyurethane mold that has positive microfluidic patterns of aspiration channel and cell delivery channel. It was mechanically detached from the mold. The detached microfluidic devices were bonded to a 2 μm-thick PDMS membrane using O_2 plasma. As a result, the inside of the microfluidic networks were sealed. After pre-cured PDMS was poured on top of the sealed microfluidic device and set in a vacuum

chamber, vacuum and heat was applied at the same time in order to minimize time needed for the process and also to fix the channel shape when it is fully expanded. Vacuum expansion process longer than 30 minutes without full curing decreased the amount of expansion since PDMS is air-permeable. The vacuum chamber was built in aluminum and connected to a vacuum pump using heat-resistant tube. Heat-resistant O-ring was used to seal the gap between the aluminum container and the lid during the vacuum expansion process.

As the pressure in the chamber drops, the pressure difference between the inside and outside of the microfluidic channels increases and the inside volume of the microchannels is expanded. The expansion mainly occurred on the 2 μm-thick PDMS membrane side of the channel. The flat 2 μm-thick sidewall was transformed to a dome shape as shown schematically in Figure 2.9 (c). The PDMS device was kept in the vacuum chamber for 12 minutes at 140℃ for cross-linking. After the cross-linking process, the dome shape of the microfluidic channels was fixed. Each individual device was cut and punched for fluidic connections from outside. Figure 2.12 shows the microscopic image and the cross sectional view of the vacuum expanded channels.

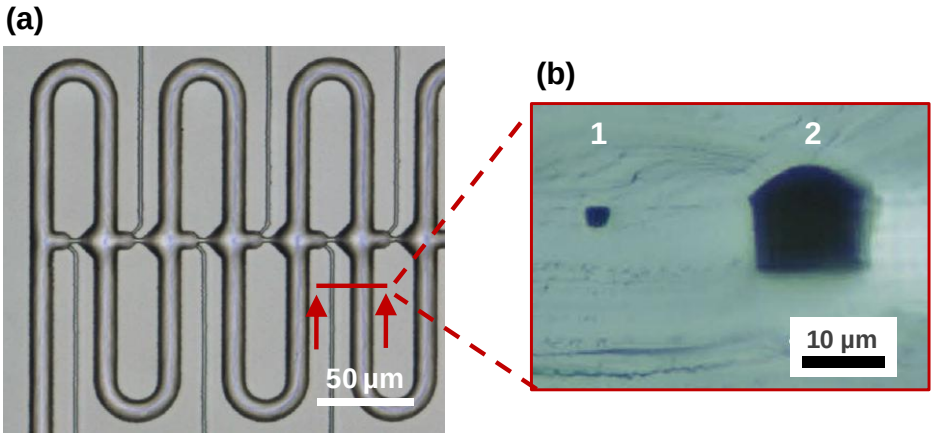

Figure 2.12 (a) Microscopic image of the vacuum expanded microchannel (b) Cross-sectional view of the vacuum expanded microchannel. Cell delivery channel (2) was expanded but aspiration channel (1) was not.

After the transformation into a dome shape sidewall, the main channel and the trapping channel result in different cross-sections, depending on their sizes of the original rectangle cross-section. With a PDMS membrane of fixed thickness, the larger cross-sectional area of the channels causes the larger transformation into the dome shape. In our cell trapping applications, the cross-sectional area of the trapping channel 3 µm x 3 µm, which is much smaller than the 9 µm x 19 µm area of the cell delivery channel. Thus, the shape of the aspiration channel remains virtually unchanged, while that of the cell delivery and trapping channels convert into a dome shape. This difference in the transformation also influences the relative position of the junction. The junction was originally located at the edge of the sidewalls. After the transformation, the edge gets flattened and a new extended sidewall of the dome is formed. As a result, the junction is located relatively in the middle of the extended sidewall as shown in Figure 1.4 (b) and

2.9 (c). The transformed raised junction has a major impact on micropipette aspiration application as schematically shown in Figure 1.4 (b). When a cell was trapped at the on-plane junction, there was a large gap caused by the asymmetries in the location and the shape of the on-plane junction and it needed to deform its shape to be completely trapped. However, at the vacuum expanded junction, these asymmetries are much reduced and a cell can be effectively trapped without the large deformation of the shape. In addition, the trapped cell experiences more uniformly distributed trapping stress on its cellular membrane and it has more possibility to preserve its cell dynamics such as membrane integrity, mechanical responses and chemical responses. Thus suction pressure and cell elongation can be measured more accurately.

CHAPTER III

CHARACTERIZATION OF MECHANICAL PROPERTIES OF CANCER CELLS USING THE MICRO-ASPIRATOR CHIP

3.1 Cell Preparation

Device operation was demonstrated using HeLa cells which is derived from cervical cancer cells. HeLa cells were obtained from Dr. Jayaraman's lab at the Department of Chemical Engineering, Texas A&M University (College Station, TX). These cell lines were maintained in accordance with the American Type Culture Collection (ATCC) guidelines [80]. Cells were cultured in 37°C, 5% CO_2, and 95% humidity environment till 80%-90% confluency in Dulbecco's Modified Eagle's Medium (DMEM, Invitrogen Corp., Carlsbad, CA) with 10% Bovine Serum (BS, Invitrogen Corp., Carlsbad, CA). To harvest the cells, the cells are first rinsed with Phosphate-Buffered Saline (Dulbecco's PBS, Invitrogen Corp., Carlsbad, CA) and then incubated in 0.25% Trypsin (Invitrogen Corp., Carlsbad, CA) for 3 min at 37°C. DMEM with BS is added to neutralize the Trypsin. The cells are then aspirated and centrifuged for 5 min at 800 rpm (Eppendorf Centrifuge, Eppendorf Co., Hauppauge, NY). After the centrifugation, the media is replaced with PBS solution and the cells are ready to use. The cell concentration in the suspension is around 1×10^6 cells ml^{-1}. Details about cell culture are described in Appendix E.

3.2 Set-up and Device Operation

The experimental system is shown schematically in Figure 3.1. Before starting the experiment, all microchannels of the micro-aspirator chip including the cell delivery channels and the aspiration channels were filled with PBS. HeLa cell suspension was prepared in 1 mL syringe and connected to the inlet of the cell delivery channel using silicon tubing. After installing the micro-aspirator chip on the inverted microscopic stage, the reservoir was connected to the outlet of the aspiration channel with silicon tubing. HeLa cell suspension was injected into the microfluidic cell delivery channel by manually pressing the syringe to capture the cells inside the traps. The outlet of the cell delivery channel was left open so we can consider the pressure inside the cell delivery channel after cell loading same as atmospheric pressure.

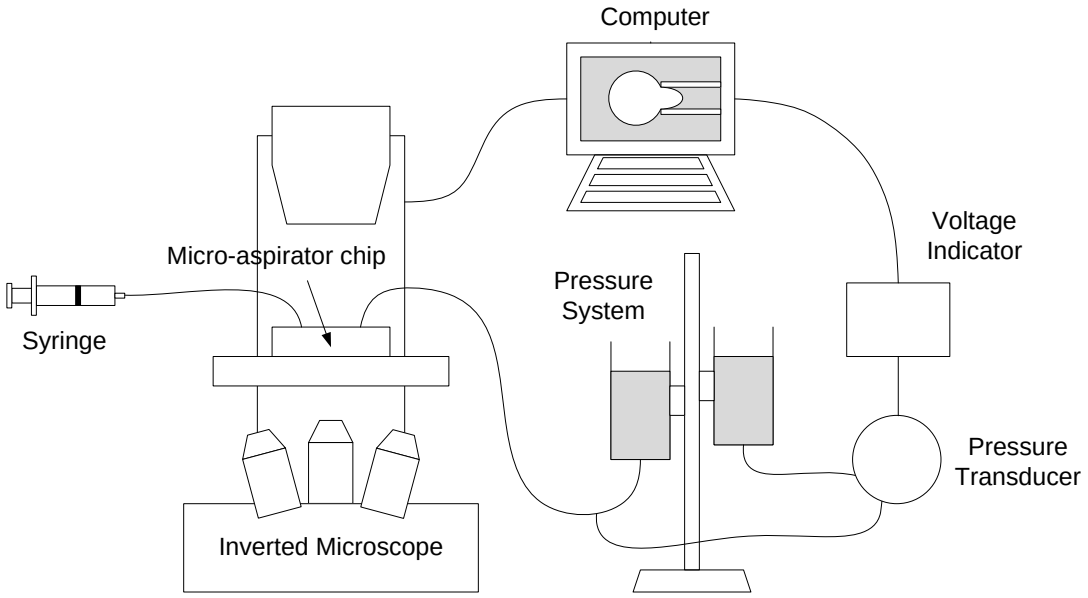

Figure 3.1 Schematic diagram of the experimental set-up.

The pressure system is composed of a large volume reservoir, a pressure transducer and a voltage indicator. The reservoir was partially filled with PBS and connected to the micro-aspirator chip through the silicon tubing. The pressure was controlled by adjusting the height of the PBS level at the end of the reservoir. A part of the line between the micro-aspirator chip and the reservoir is connected to a pressure transducer (PX82B0-005D5V, Omega Engineering Inc., Stamford, CT). In order to measure the actual suction pressure applied to the cells, the T-joint was placed near the micro-aspirator chip as close as possible. The voltage signal from the pressure transducer was measured using voltage indicator (DP41-E, Omega Engineering Inc., Stamford, CT) and acquired using LabVIEW^{TM}. VISA library was used for RS-232 serial cable communication. LabVIEW^{TM} front panel and block diagram are shown in Appendix F. The transducer is calibrated with a water manometer before each experiment.

When a negative pressure is applied to the aspiration channels, the trapped cells are drawn into the aspiration channel. Conventional micropipette aspiration technique needs slight adjustment of pressure to maintain the cell in its initial position before the aspiration experiment. But since the micro-aspirator chip can capture the cells into the traps where the aspiration channel is connected, this cell positioning step was not required. Following the cell trapping, 6 steps of suction pressure between 1-6 kPa were applied using a height-adjustable, reservoir pressure source, and the aspiration length of HeLa cells was measured. All processes were observed through an inverted microscope (Eclipse TS100, Nikon Instruments Inc., Melville, NY) and recorded using CCD camera

(Digital Sight DS-2 Mv, Nikon Instruments Inc., Melville, NY). Cell experiment was performed at room temperature, i.e., 22-24°C.

3.3 Results and Discussion

3.3.1 Trapping HeLa Cells

After installing the micro-aspirator chip on the inverted microscopic stage and connecting to pressure system, HeLa cell suspension was manually injected into the cell delivery channel with 40 cell traps using a syringe. Figure 3.2 shows the overall image of the microchannels of the micro-aspirator chip and the image of HeLa cells captured inside arrays of cell traps. As shown in Figure 3.3, we could observe that the cells were trapped in order just like the result of the preliminary test using the 90 μm diameter microbeads.

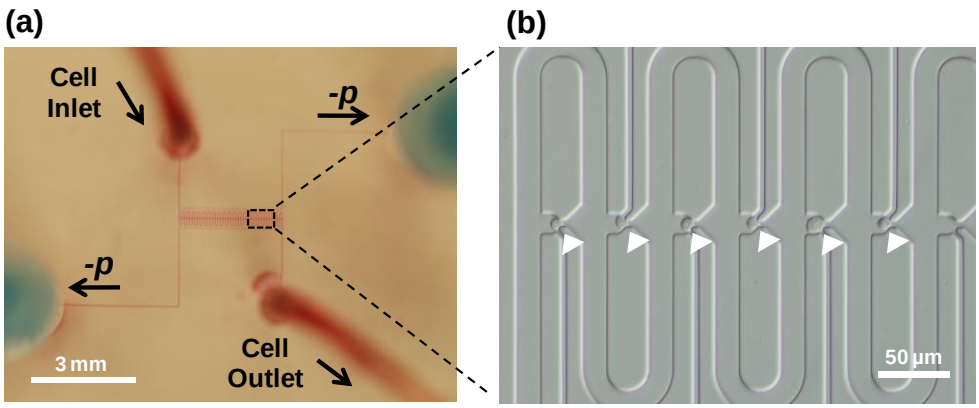

Figure 3.2 (a) Image of the micro-aspirator chip. Red color dye was used to show the shape of microchannels. Aspiration channel tube was filled with blue color dye. (b) Microscopic image of single cells captured inside arrays of cell traps. White arrow heads indicate the cells trapped.

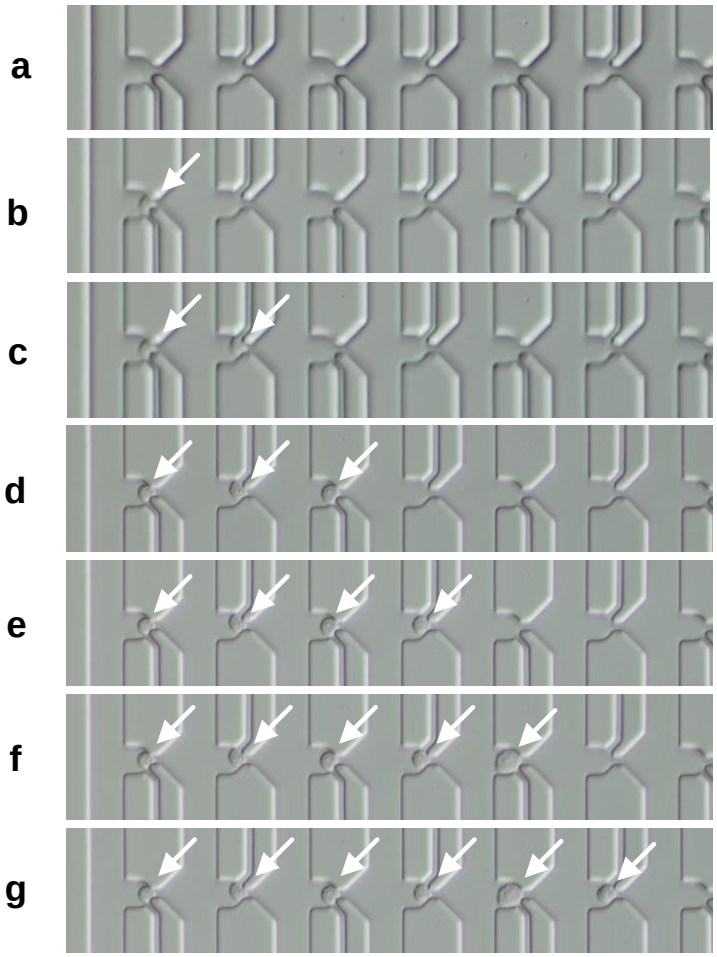

Figure 3.3 Microscopic images of cell trapping. HeLa cells were trapped in order. White arrows indicate the cells trapped.

3.3.2 Stiffness of HeLa Cells

Three devices were used to demonstrate the performance and repeatability of the micro-aspirator chip. Following cell trapping, 6 steps of suction pressure from 1 to 6 kPa was applied by lowering the reservoir pressure source. As same as the principle of manometer, 10 cm height difference caused approximately 1 kPa of suction pressure.

Since it took approximately 1-3 minutes for the cells to reach the fully aspirated state (data not shown), suction pressure was increased step by step with an interval of 3 min. Figure 3.4 shows the microscopic images of HeLa cell gradually aspirated into the aspiration channel depending on the amount of suction pressure applied.

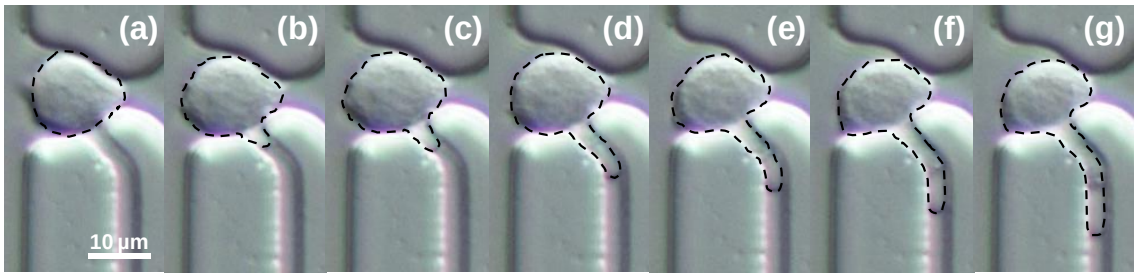

Figure 3.4 HeLa cell aspirated at suction pressure (a) 0 kPa, (b) 1 kPa, (c) 2 kPa, (d) 3 kPa, (e) 4 kPa, (f) 5 kPa and (g) 6 kPa. Time intervals of the images were 3 min.

The aspiration length of the cells at each pressure applied was measured using the microscopic images (Eclipse TS100, Nikon Instruments Inc., Melville, NY). Figure 3.5 shows the result of the experiments using 3 devices. As shown in Figure 3.5 (a), linear trend between the suction pressure applied and the aspiration length was observed in all channels of 3 devices. The application of a step increase in pressure caused step increase in the aspiration length and the distance that the cell entered the aspiration channel was up to 2-6 times the radius of the aspiration channel. This shows that HeLa cells exhibited solid like behavior in response to a step increase in pressure. From the slope of the trend line for each cell, Young's modulus was calculated based on Theret et

al.'s model [31]. HeLa cell Young's modulus of 1.3 ± 1.0 kPa (n = 17), 1.1 ± 0.5 kPa (n = 18) and 1.5 ± 0.7 kPa (n = 19) were obtained for device 1, 2 and 3 respectively. The cells not aspirated were excluded for the calculation.

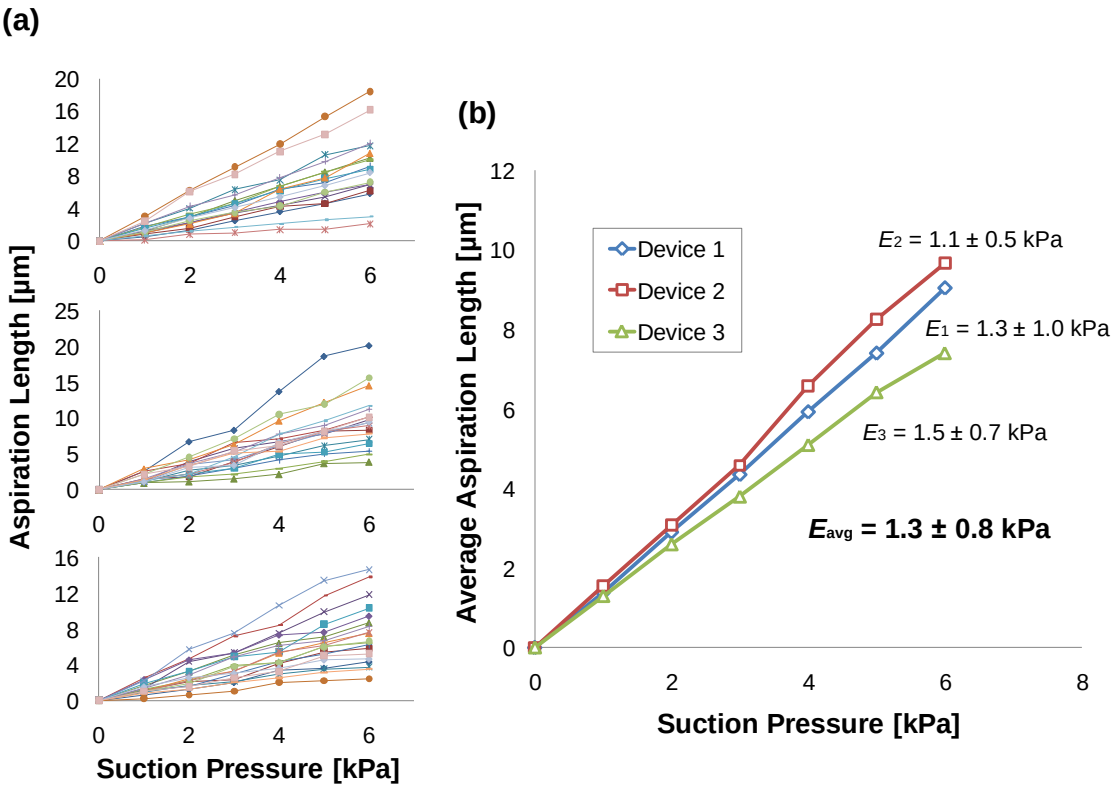

Figure 3.5 Suction pressure vs. aspiration length of HeLa cells. (a) Linear trend between the suction pressure applied and the aspiration length was observed in all channels of 3 devices. (b) The average aspiration length of 3 devices was compared to show the repeatability of the micro-aspirator chip.

The average Young's modulus of all 54 cells was 1.3 ± 0.8 kPa (n = 54). This is at the lower range of previously reported HeLa cell Young's modulus. This might be due to the square geometry of the aspiration channel resulting in deviation from the true

Young's modulus, as well as from the variation in cell conditions and experimental procedures in various reports. Table 3.1 shows the HeLa cell Young's modulus previously reported and obtained in this work.

Table 3.1 Comparison of Young's modulus of HeLa cell measured using various methods.

Cell type	Young's modulus (kPa)	Method	Reference
HeLa	1.8 ± 0.8 (nucleus) 5.1 ± 1.4 (cell peripheries)	Atomic Force Microscopy (AFM)	Yokokawa *et al.* 2008 [81]
HeLa	50-500	AFM	Gigler *et al.* 2007 [82]
HeLa	100-200	AFM	Leporatti *et al.* 2009 [83]
HeLa	0.25	Magnetic tweezers	De Vries *et al.* 2007 [84]
HeLa	1.3 ± 0.8	Microfluidic Micropipette Aspiration	Kim *et al.* 2010 (This work)

As previously mentioned in Chapter I, in Theret *et al.*'s half-space model, cells were considered as homogeneous elastic material to simplify the analysis model. But in reality, biological cell contains a nucleus as well as a variety of organelles and cytoskeletal elements which course through the entire cytoplasmic volume.

The cytoskeleton is a network of filaments that helps to define a cell's shape. The thinnest of the filaments are actin filaments. The thickest filaments are called microtubules because they have the form of minute hollow tubes. Intermediate in thickness between actin filaments and microtubules are the intermediate filaments. These three types of filaments, together with other proteins that attach to them, form a system of girders, ropes, and motors that gives the cell its mechanical strength and

controls its shape. Previous researches have shown that disruption of the cytoskeleton contributes to a weakening, i.e., a decrease in the cell mechanical properties [10, 85].

Various inhibitors can be used to verify the main component that determines the stiffness of the cell in micropipette aspiration. For example, phalloidin which inhibits disassembly of the actin filaments or cytochalasin which inhibits assembly of the actin filaments can be used to see how polymerization or depolymerization of actin filaments is related to the stiffness of the cells. Myosin inhibitor 2,3-Butanedione monoxime (BDM) can be used to verify the role of myosin.

3.3.3 Repeatability of the Devices

In Figure 3.5 (b), the average aspiration length of 3 devices was compared to show the repeatability of the micro-aspirator chip. The average and standard deviation of Young's modulus of the 3 devices was 1.3 ± 0.2 kPa (n = 3) (Table 3.2). Although the standard deviation of Young's modulus of each channel of the device was high (75.1%, 45.0% and 48.6% respectively), that of 3 devices was much lower (15.2%) representing good repeatability of the devices and the system.

Table 3.2 Repeatability test of the devices using HeLa cells.

Device #	N	Cell Diameter [μm]			Young's Modulus [kPa]		
		Ave	SD	RSD [%]	Ave	SD	RSD [%]
Device 1	17	15.0	1.7	11.0	1.3	1.0	75.1
Device 2	18	15.4	2.0	13.3	1.1	0.5	45.0
Device 3	19	15.5	2.0	12.8	1.5	0.7	48.6
All devices	3	15.3	0.2	1.6	1.3	0.2	15.2

3.3.4 Size of HeLa Cells vs. Stiffness

Diameter of each cell was obtained based on circumference measured using microscopic images before applying suction pressure. Linear correlation analysis was performed to investigate trends in the cell stiffness versus the cell size (diameter). As shown in Figure 3.6, there was no dependence of the modulus on the cell diameter.

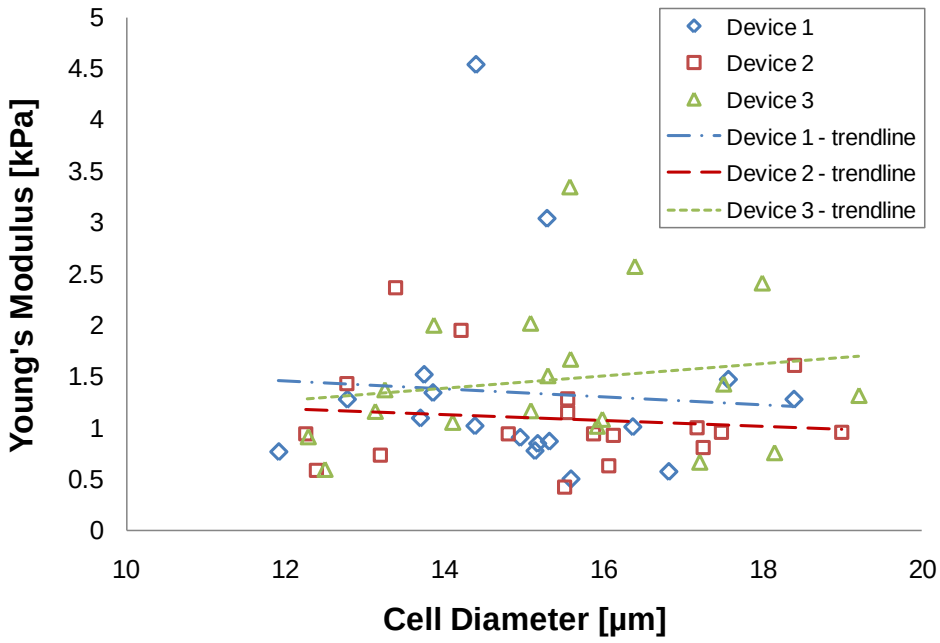

Figure 3.6 Correlation between the Young's modulus and the cell diameter. No significant correlation was observed, suggesting that the geometry of the test configuration did not influence the stiffness.

CHAPTER IV

CONCLUSION AND FUTURE WORK

Recent researches report that the mechanical properties of cells could be used as indicators of its biological state, offering valuable insights into the pathogenic basis of diseases, including the possible identification of one disease from another [10, 85]. The cytoskeleton - the internal scaffolding comprising a complex network of biopolymeric molecules - is known to determine the cell's shape and mechanical deformation characteristics [10, 85]. However, existing micropipette aspiration techniques are not capable of quantifying mechanical parameters of biological cells in statistically significant quantities.

In order to address these limitations, a micro-aspirator chip system that can aspirate and measure the deformation of 20 cells simultaneously was developed and characterized. A micro-aspirator chip system can aspirate and measure the deformation of 20 cells simultaneously. The system was fabricated using combinations of conventional microfabrication techniques and PDMS membrane vacuum expansion techniques. For the PDMS microfluidic layer part, fabrication techniques such as photolithography and soft lithography were used. In order to make semicircular cell trap, 2 μm-thick PDMS membrane was self-raised through vacuum expansion process.

The principle of cell trapping is based on differences in flow resistance inside the microfluidic channels. After all traps are filled with cells, negative pressure can be applied to the aspiration channel using hydrostatic pressure. One of the key design

concepts of this device is the aspiration channel positioned at the center of the cell both in vertical and horizontal direction to obtain a good seal just like a traditional micropipette.

Device operation was demonstrated using HeLa cells. The cell trapping efficiency was almost 100%. Using this device, Young's modulus of 1.3 ± 0.8 kPa (n = 54) was obtained for HeLa cells. Device to device variation was less than 15.2% (n = 3), showing good repeatability of the device. No dependence of the Young's modulus on the cell diameter was found.

In conclusion, a high-throughput micro-aspirator chip, which can deliver, trap, and deform multiple cells simultaneously with single-cell resolution without skill-dependent micromanipulation was developed and demonstrated. This system can improve characterization throughput over traditional micropipette aspiration to obtain statistically significant quantities of data, and thus, enabling the evaluation of mechanical stiffness as a marker for cell type and condition.

Some of the future work is listed. In order to obtain accurate Young's modulus using this system, analytical model of micropipette aspiration with square geometry needs to be developed. Repeated studies with different cell lines would provide further information about the performance of the system. Especially, the cell type which has inherent round shape such as leukocyte would be of great interest. In addition, pre-treatment of the cell using chemical inhibitors might lead to a better understanding of the components inside the cells which determine the cell stiffness.

REFERENCES

[1] R. M. Hochmuth, "Micropipette aspiration of living cells," *J Biomech,* vol. 33, pp. 15-22, Jan 2000.

[2] D. B. Weibel, W. R. Diluzio, and G. M. Whitesides, "Microfabrication meets microbiology," *Nat Rev Microbiol,* vol. 5, pp. 209-18, Mar 2007.

[3] Y. Xia and G. M. Whitesides, "Soft lithography," *Angewandte Chemie, International Edition,* vol. 37, pp. 550-575, 1998.

[4] H. W. Hou, Q. S. Li, G. Y. Lee, A. P. Kumar, C. N. Ong, and C. T. Lim, "Deformability study of breast cancer cells using microfluidics," *Biomed Microdevices,* vol. 11, pp. 557-64, Jun 2009.

[5] W. G. Lee, H. Bang, H. Yun, J. Lee, J. Park, J. K. Kim, S. Chung, K. Cho, C. Chung, D. C. Han, and J. K. Chang, "On-chip erythrocyte deformability test under optical pressure," *Lab Chip,* vol. 7, pp. 516-9, Apr 2007.

[6] J. P. Shelby, J. White, K. Ganesan, P. K. Rathod, and D. T. Chiu, "A microfluidic model for single-cell capillary obstruction by Plasmodium falciparum-infected erythrocytes," *Proc Natl Acad Sci U S A,* vol. 100, pp. 14618-22, Dec 9 2003.

[7] C. Moraes, J. Tong, X.Y. Liu, C.A. Simmons, and Y. Sun, "Parallel micropipette aspirator arrays for high-throughput mechanical characterization of biological cells," *in Proc. MicroTAS 2007,* pp. 751-753.

[8] WHO. (2010, Jun). *Quick cancer facts*. Available: www.who.int/cancer/en/

[9] WHO, *Guidelines for the treatment of malaria, second edition*, 2010.

[10] G. Bao and S. Suresh, "Cell and molecular mechanics of biological materials," *Nat Mater,* vol. 2, pp. 715-25, Nov 2003.

[11] S. Kasas and G. Dietler, "Probing nanomechanical properties from biomolecules to living cells," *Pflugers Arch,* vol. 456, pp. 13-27, Apr 2008.

[12] S. E. Cross, Y. S. Jin, J. Rao, and J. K. Gimzewski, "Nanomechanical analysis of cells from cancer patients," *Nat Nanotechnol,* vol. 2, pp. 780-3, Dec 2007.

[13] D. E. Discher, P. Janmey, and Y. L. Wang, "Tissue cells feel and respond to the stiffness of their substrate," *Science,* vol. 310, pp. 1139-43, Nov 18 2005.

[14] S. Suresh, "Biomechanics and biophysics of cancer cells," *Acta Biomater,* vol. 3, pp. 413-38, Jul 2007.

[15] G. Y. Lee and C. T. Lim, "Biomechanics approaches to studying human diseases," *Trends Biotechnol,* vol. 25, pp. 111-8, Mar 2007.

[16] G. B. Nash, C. S. Johnson, and H. J. Meiselman, "Mechanical properties of oxygenated red blood cells in sickle cell (HbSS) disease," *Blood,* vol. 63, pp. 73-82, Jan 1984.

[17] D. E. Ingber, "Mechanobiology and diseases of mechanotransduction," *Ann Med,* vol. 35, pp. 564-77, 2003.

[18] J. Guck, S. Schinkinger, B. Lincoln, F. Wottawah, S. Ebert, M. Romeyke, D. Lenz, H. M. Erickson, R. Ananthakrishnan, D. Mitchell, J. Kas, S. Ulvick, and C. Bilby, "Optical deformability as an inherent cell marker for testing malignant transformation and metastatic competence," *Biophys J,* vol. 88, pp. 3689-98, May 2005.

[19] T. D. Pollard and G. G. Borisy, "Cellular motility driven by assembly and disassembly of actin filaments," *Cell,* vol. 112, pp. 453-65, Feb 21 2003.

[20] P. F. Davies, "Flow-mediated endothelial mechanotransduction," *Physiol Rev,* vol. 75, pp. 519-60, Jul 1995.

[21] A. S. French, "Mechanotransduction," *Annu Rev Physiol,* vol. 54, pp. 135-52, 1992.

[22] A. Han, L. Yang, and A. B. Frazier, "Quantification of the heterogeneity in breast cancer cell lines using whole-cell impedance spectroscopy," *Clin Cancer Res,* vol. 13, pp. 139-43, Jan 1 2007.

[23] J. M. Mitchison and M. M. Swann, "The mechanical properties of the cell surface," *J Exp Biol,* vol. 31, pp. 97-104, 1954.

[24] R. P. Rand and A. C. Burton, "Mechanical properties of the red cell membrane. I. Membrane stiffness and intracellular pressure," *Biophys J,* vol. 4, pp. 115-35, Mar 1964.

[25] E. A. Evans and R. M. Hochmuth, "Membrane viscoelasticity," *Biophys J,* vol. 16, pp. 1-11, Jan 1976.

[26] S. Chien, G. W. Schmid-Schonbein, K. L. Sung, E. A. Schmalzer, and R. Skalak, "Viscoelastic properties of leukocytes," *Kroc Found Ser,* vol. 16, pp. 19-51, 1984.

[27] E. A. Evans, "Bending elastic modulus of red blood cell membrane derived from buckling instability in micropipet aspiration tests," *Biophys J,* vol. 43, pp. 27-30, Jul 1983.

[28] F. J. Byfield, H. Aranda-Espinoza, V. G. Romanenko, G. H. Rothblat, and I. Levitan, "Cholesterol depletion increases membrane stiffness of aortic endothelial cells," *Biophys J,* vol. 87, pp. 3336-43, Nov 2004.

[29] E. Evans and A. Yeung, "Apparent viscosity and cortical tension of blood granulocytes determined by micropipet aspiration," *Biophys J,* vol. 56, pp. 151-60, Jul 1989.

[30] W. R. Jones, H. P. Ting-Beall, G. M. Lee, S. S. Kelley, R. M. Hochmuth, and F. Guilak, "Alterations in the Young's modulus and volumetric properties of chondrocytes isolated from normal and osteoarthritic human cartilage," *J Biomech,* vol. 32, pp. 119-27, Feb 1999.

[31] D. P. Theret, M. J. Levesque, M. Sato, R. M. Nerem, and L. T. Wheeler, "The application of a homogeneous half-space model in the analysis of endothelial cell micropipette measurements," *J Biomech Eng,* vol. 110, pp. 190-9, Aug 1988.

[32] G. Binnig, C. F. Quate, and C. Gerber, "Atomic force microscope," *Phys Rev Lett,* vol. 56, p. 930, 1986.

[33] V. Shahin and N. P. Barrera, "Providing unique insight into cell biology via atomic force microscopy," *Int Rev Cytol,* vol. 265, pp. 227-52, 2008.

[34] L. P. Silva, "Imaging proteins with atomic force microscopy: an overview," *Curr Protein Pept Sci,* vol. 6, pp. 387-95, Aug 2005.

[35] D. J. Muller, "AFM: a nanotool in membrane biology," *Biochemistry,* vol. 47, pp. 7986-98, Aug 5 2008.

[36] A. Engel and H. E. Gaub, "Structure and mechanics of membrane proteins," *Annu Rev Biochem,* vol. 77, pp. 127-48, 2008.

[37] H. G. Hansma, K. Kasuya, and E. Oroudjev, "Atomic force microscopy imaging and pulling of nucleic acids," *Curr Opin Struct Biol,* vol. 14, pp. 380-5, Jun 2004.

[38] Y. Hirano, H. Takahashi, M. Kumeta, K. Hizume, Y. Hirai, S. Otsuka, S. H. Yoshimura, and K. Takeyasu, "Nuclear architecture and chromatin dynamics revealed by atomic force microscopy in combination with biochemistry and cell biology," *Pflugers Arch,* vol. 456, pp. 139-53, Apr 2008.

[39] D. Pesen and J. H. Hoh, "Micromechanical architecture of the endothelial cell cortex," *Biophys J,* vol. 88, pp. 670-9, Jan 2005.

[40] C. Rotsch, K. Jacobson, and M. Radmacher, "Dimensional and mechanical dynamics of active and stable edges in motile fibroblasts investigated by using atomic force microscopy," *Proc Natl Acad Sci U S A,* vol. 96, pp. 921-6, Feb 2 1999.

[41] U. G. Hofmann, C. Rotsch, W. J. Parak, and M. Radmacher, "Investigating the cytoskeleton of chicken cardiocytes with the atomic force microscope," *J Struct Biol,* vol. 119, pp. 84-91, Jul 1997.

[42] C. Rotsch, F. Braet, E. Wisse, and M. Radmacher, "AFM imaging and elasticity measurements on living rat liver macrophages," *Cell Biol Int,* vol. 21, pp. 685-96, Nov 1997.

[43] C. Rotsch and M. Radmacher, "Drug-induced changes of cytoskeletal structure and mechanics in fibroblasts: an atomic force microscopy study," *Biophys J,* vol. 78, pp. 520-35, Jan 2000.

[44] J. Solon, I. Levental, K. Sengupta, P. C. Georges, and P. A. Janmey, "Fibroblast adaptation and stiffness matching to soft elastic substrates," *Biophys J,* vol. 93, pp. 4453-61, Dec 15 2007.

[45] E. Takai, K. D. Costa, A. Shaheen, C. T. Hung, and X. E. Guo, "Osteoblast elastic modulus measured by atomic force microscopy is substrate dependent," *Ann Biomed Eng,* vol. 33, pp. 963-71, Jul 2005.

[46] A. M. Collinsworth, S. Zhang, W. E. Kraus, and G. A. Truskey, "Apparent elastic modulus and hysteresis of skeletal muscle cells throughout differentiation," *Am J Physiol Cell Physiol,* vol. 283, pp. C1219-27, Oct 2002.

[47] A. J. Engler, M. A. Griffin, S. Sen, C. G. Bonnemann, H. L. Sweeney, and D. E. Discher, "Myotubes differentiate optimally on substrates with tissue-like stiffness: pathological implications for soft or stiff microenvironments," *J Cell Biol,* vol. 166, pp. 877-87, Sep 13 2004.

[48] W. A. Lam, M. J. Rosenbluth, and D. A. Fletcher, "Chemotherapy exposure increases leukemia cell stiffness," *Blood,* vol. 109, pp. 3505-8, Apr 15 2007.

[49] M. J. Rosenbluth, W. A. Lam, and D. A. Fletcher, "Force microscopy of nonadherent cells: a comparison of leukemia cell deformability," *Biophys J,* vol. 90, pp. 2994-3003, Apr 15 2006.

[50] Z. Lu, Z. Zhang, and D. Pang, "Atomic force microscopy in cell biology," *Chinese Science Bulletin,* vol. 50, pp. 1409-1414 2005.

[51] A. V. Bolshakova, O. I. Kiselyova, A. S. Filonov, O. Y. Frolova, Y. L. Lyubchenko, and I. V. Yaminsky, "Comparative studies of bacteria with an atomic force microscopy operating in different modes," *Ultramicroscopy,* vol. 86, pp. 121-8, Jan 2001.

[52] M. Micic, D. Hu, Y. D. Suh, G. Newton, M. Romine, and H. P. Lu, "Correlated atomic force microscopy and fluorescence lifetime imaging of live bacterial cells," *Colloids Surf B Biointerfaces,* vol. 34, pp. 205-12, Apr 15 2004.

[53] G. M. Whitesides, "The origins and the future of microfluidics," *Nature,* vol. 442, pp. 368-73, Jul 27 2006.

[54] G. M. Whitesides, E. Ostuni, S. Takayama, X. Jiang, and D. E. Ingber, "Soft lithography in biology and biochemistry," *Annu Rev Biomed Eng,* vol. 3, pp. 335-73, 2001.

[55] J. N. Lee, X. Jiang, D. Ryan, and G. M. Whitesides, "Compatibility of mammalian cells on surfaces of poly(dimethylsiloxane)," *Langmuir,* vol. 20, pp. 11684-91, Dec 21 2004.

[56] S. Takayama, E. Ostuni, P. LeDuc, K. Naruse, D. E. Ingber, and G. M. Whitesides, "Selective chemical treatment of cellular microdomains using multiple laminar streams," *Chem Biol,* vol. 10, pp. 123-30, Feb 2003.

[57] H. Lu, L. Y. Koo, W. M. Wang, D. A. Lauffenburger, L. G. Griffith, and K. F. Jensen, "Microfluidic shear devices for quantitative analysis of cell adhesion," *Anal Chem,* vol. 76, pp. 5257-64, Sep 15 2004.

[58] B. S. Cho, T. G. Schuster, X. Zhu, D. Chang, G. D. Smith, and S. Takayama, "Passively driven integrated microfluidic system for separation of motile sperm," *Anal Chem,* vol. 75, pp. 1671-5, Apr 1 2003.

[59] M. A. McClain, C. T. Culbertson, S. C. Jacobson, N. L. Allbritton, C. E. Sims, and J. M. Ramsey, "Microfluidic devices for the high-throughput chemical analysis of cells," *Anal Chem,* vol. 75, pp. 5646-55, Nov 1 2003.

[60] H. Kiesewetter, U. Dauer, P. Teitel, H. Schmid-Schonbein, and R. Trapp, "The single erythrocyte rigidometer (SER) as a reference for RBC deformability," *Biorheology,* vol. 19, pp. 737-53, 1982.

[61] R. S. Frank and R. M. Hochmuth, "An investigation of particle flow through capillary models with the resistive pulse technique," *J Biomech Eng,* vol. 109, pp. 103-9, May 1987.

[62] M. J. Rosenbluth, W. A. Lam, and D. A. Fletcher, "Analyzing cell mechanics in hematologic diseases with microfluidic biophysical flow cytometry," *Lab Chip,* vol. 8, pp. 1062-70, Jul 2008.

[63] A. Y. Lau, P. J. Hung, A. R. Wu, and L. P. Lee, "Open-access microfluidic patch-clamp array with raised lateral cell trapping sites," *Lab Chip,* vol. 6, pp. 1510-5, Dec 2006.

[64] J. Seo and L. P. Lee, "Self-raised circular orifices for lateral patch-clamping array chips," *in Proc. MicroTAS 2005,* pp. 1215-1217.

[65] A. Khademhosseini, J. Yeh, S. Jon, G. Eng, K. Y. Suh, J. A. Burdick, and R. Langer, "Molded polyethylene glycol microstructures for capturing cells within microfluidic channels," *Lab Chip,* vol. 4, pp. 425-30, Oct 2004.

[66] S. Kobel, M. Limacher, S. Gobaa, T. Laroche, and M. P. Lutolf, "Micropatterning of hydrogels by soft embossing," *Langmuir,* vol. 25, pp. 8774-9, Aug 4 2009.

[67] A. O. Ogunniyi, C. M. Story, E. Papa, E. Guillen, and J. C. Love, "Screening individual hybridomas by microengraving to discover monoclonal antibodies," *Nat Protoc,* vol. 4, pp. 767-82, 2009.

[68] J. Nilsson, M. Evander, B. Hammarstrom, and T. Laurell, "Review of cell and particle trapping in microfluidic systems," *Anal Chim Acta,* vol. 649, pp. 141-57, Sep 7 2009.

[69] J. Seo, C. Ionescu-Zanetti, J. Diamond, R. Lal, and L. P. Lee, "Integrated multiple patch-clamp array chip via lateral cell trapping junctions," *Applied Physics Letters,* vol. 84, pp. 1973-1975, 2004.

[70] M. Khine, A. Lau, C. Ionescu-Zanetti, J. Seo, and L. P. Lee, "A single cell electroporation chip," *Lab Chip,* vol. 5, pp. 38-43, Jan 2005.

[71] P.J. Lee, P.J. Hung, R. Shaw, L. Jan, and L. P. Lee, "Microfluidic application integrated device for monitoring direct cell-cell communication via gap junctions between individual cell pairs," *Applied Physics Letters,* vol. 86, 2005.

[72] A. Valero, J. N. Post, J. W. van Nieuwkasteele, P. M. Ter Braak, W. Kruijer, and A. van den Berg, "Gene transfer and protein dynamics in stem cells using single cell electroporation in a microfluidic device," *Lab Chip,* vol. 8, pp. 62-7, Jan 2008.

[73] D. Di Carlo, L. Y. Wu, and L. P. Lee, "Dynamic single cell culture array," *Lab Chip,* vol. 6, pp. 1445-9, Nov 2006.

[74] S. Faley, K. Seale, J. Hughey, D. K. Schaffer, S. VanCompernolle, B. McKinney, F. Baudenbacher, D. Unutmaz, and J. P. Wikswo, "Microfluidic platform for real-time signaling analysis of multiple single T cells in parallel," *Lab Chip,* vol. 8, pp. 1700-12, Oct 2008.

[75] A. R. Wheeler, W. R. Throndset, R. J. Whelan, A. M. Leach, R. N. Zare, Y. H. Liao, K. Farrell, I. D. Manger, and A. Daridon, "Microfluidic device for single-cell analysis," *Anal Chem,* vol. 75, pp. 3581-6, Jul 15 2003.

[76] D. Di Carlo, N. Aghdam, and L. P. Lee, "Single-cell enzyme concentrations, kinetics, and inhibition analysis using high-density hydrodynamic cell isolation arrays," *Anal Chem,* vol. 78, pp. 4925-30, Jul 15 2006.

[77] W. H. Tan and S. Takeuchi, "A trap-and-release integrated microfluidic system for dynamic microarray applications," *Proc Natl Acad Sci U S A,* vol. 104, pp. 1146-51, Jan 23 2007.

[78] S. Kobel, A. Valero, J. Latt, P. Renaud, and M. Lutolf, "Optimization of microfluidic single cell trapping for long-term on-chip culture," *Lab Chip,* vol. 10, pp. 857-63, Apr 7 2010.

[79] S. P. Desai, D. M. Freeman, and J. Voldman, "Plastic masters-rigid templates for soft lithography," *Lab Chip,* vol. 9, pp. 1631-7, Jun 7 2009.

[80] ATCC. (2010, Feb). *Product Description - HeLa*. Available: http://www.atcc.org

[81] M. Yokokawa, K. Takeyasu, and S. H. Yoshimura, "Mechanical properties of plasma membrane and nuclear envelope measured by scanning probe microscope," *J Microsc,* vol. 232, pp. 82-90, Oct 2008.

[82] A. Gigler, M. Holzwarth, and O. Marti, "Local nanomechanical properties of HeLa-cell surfaces," *J Phys: Conference Series,* vol. 61, pp. 780–784, 2007.

[83] S. Leporatti, D. Vergara, A. Zacheo, V. Vergaro, G. Maruccio, R. Cingolani, and R. Rinaldi, "Cytomechanical and topological investigation of MCF-7 cells by scanning force microscopy," *Nanotechnol,* vol. 20, p. 055103, Feb 4 2009.

[84] A. H. de Vries, B. E. Krenn, R. van Driel, V. Subramaniam, and J. S. Kanger, "Direct observation of nanomechanical properties of chromatin in living cells," *Nano Lett,* vol. 7, pp. 1424-7, May 2007.

[85] C. Zhu, G. Bao, and N. Wang, "Cell mechanics: mechanical response, cell adhesion, and molecular deformation," *Annu Rev Biomed Eng,* vol. 2, pp. 189-226, 2000.

APPENDIX A

MASK DESIGN

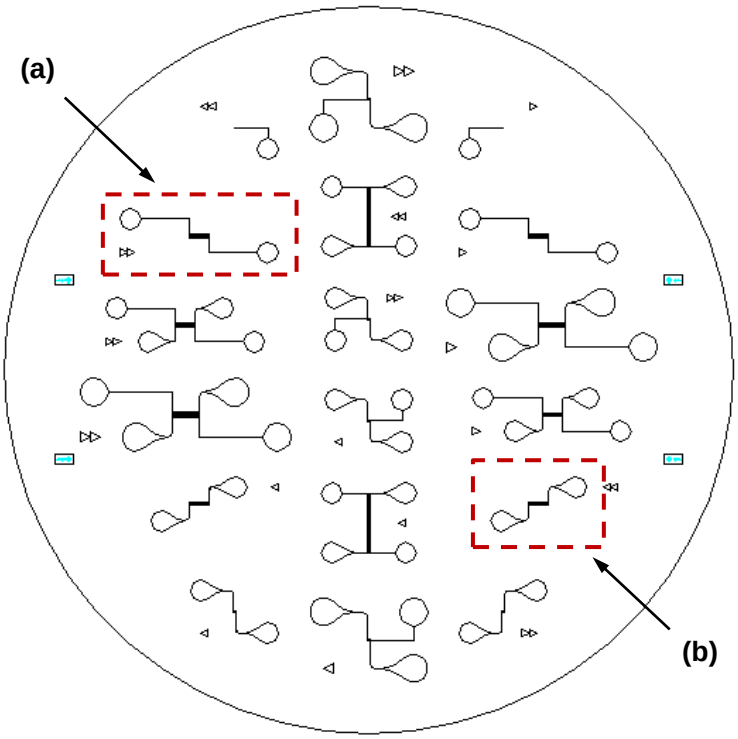

Figure A.1 Mask design. (a) Aspiration channel layer used for the micro-aspirator chip. (b) Cell delivery channel layer used for the micro-aspirator chip.

APPENDIX B

MASTER MOLD FABRICATION PROCEDURE

Aluminum alignment mark patterning procedure is as follows:

1. Prepare piranha-cleaned 3 inch silicon wafer.
2. Spin coat Microposit S1818 photoresist (Rohm and Haas Electronic Material LLC, Marlborough, MA) on the silicon wafer at 4000 rpm for 30 seconds with an acceleration time of 10 seconds.
3. Soft bake at 100°C for 10 minutes.
4. Expose UV using a mask aligner (MJB3, SUSS MicroTec Inc., Waterbury Center, VT) at 12 mW/cm^2 (wavelength: 320 nm) for 14 second with a photomask having alignment marks.
5. Post exposure bake at 130°C for 10 minutes.
6. Develop the pattern using MF-319 developer (Rohm and Haas Electronic Material LLC, Marlborough, MA) for 20-40 seconds.
7. Rinse in DI water and dry with N_2 gas. The resulting silicon wafer was covered with photoresist with only the alignment marks opened.
8. Deposit Al layer using an E-beam evaporator to a thickness of 2500 Å.
9. Sonicate the substrate in aceton, isopropyl alcohol (IPA) and DI water for 10 minutes, respectively to remove the sacrificial photoresist layer.

The fabrication step of SU-8™ master mold is as follows:

1. Spin coat 3 μm thick photoresist (SU-8™ 2002, Microchem, Inc., Newton, MA) on the alignment mark pattered silicon wafer at 750 rpm for 30 seconds.
2. Soft bake on a 95°C hotplate for 4 minutes.
3. Expose UV using a mask aligner (MA6, SUSS MicroTec Inc., Waterbury Center, VT) at 200 mJ/cm^2 with a photomask having aspiration channel patterns.
4. Post exposure bake at 95°C for 4 minutes.
5. Develop the patterns using Microposit Thinner Type P (Shipley Co., Marlborough, MA) for for 1 minute.
6. Rinse with DI water and dry with N_2 gas.
7. Spin coat 9 μm-thick photoresist (SU-8 2007™, Microchem, Inc., Newton, MA) for patterning the cell delivery channel on the silicon wafer at 2500 rpm for 25 seconds with an acceleration time of 5 seconds.
8. Soft bake at 95°C for 5 minutes.
9. Align and expose UV using a mask aligner (MA6, SUSS MicroTec Inc., Waterbury Center, VT) at 180 mJ/cm^2 with a photomask having cell delivery channel patterns.
10. Post exposure bake on a hot plate at 95°C for 5 minutes.
11. Develop the patterns using Microposit Thinner Type P (Shipley Co., Marlborough, MA) for 1 minute.
12. Rinse with DI water and dry with N_2 gas.

APPENDIX C

PDMS MEMBRANE FABRICATION PROCEDURE

PDMS membrane fabrication procedure is as follows:

1. Place 3 inch silicon wafers inside the desiccator with 2 ~ 3 drops of (tridecafluoro-1,1,2,2-tetrahydrooctyl) trichlorosilane (United Chemical Technologies, Inc., Bristol, PA) on a weight boat.
2. Apply vacuum for 15 minutes and take them out.
3. Mix PDMS (Sylgard® 184, Dow Corning, Inc., Midland, MI) in a 10 : 1 base : hardener ratio (w/w) and subsequently degassed in a vacuum chamber for 20 minutes.
4. Gently mix PDMS pre-polymer with hexane in a 1 : 3 ratio (w/w).
5. Spin coat the mixture at 4500 rpm for 30 seconds on a trichlorosilane coated silicon wafer.
6. Cure inside the oven at 85°C for 15 minutes.
7. After O_2 plasma treatment, bond the PDMS replica on the top of the PDMS membrane.
8. Peel off the PDMS replica gently and the PDMS membrane will stay bonded to the device.

APPENDIX D

PDMS MEMBRANE VACUUM EXPANSION PROCEDURE

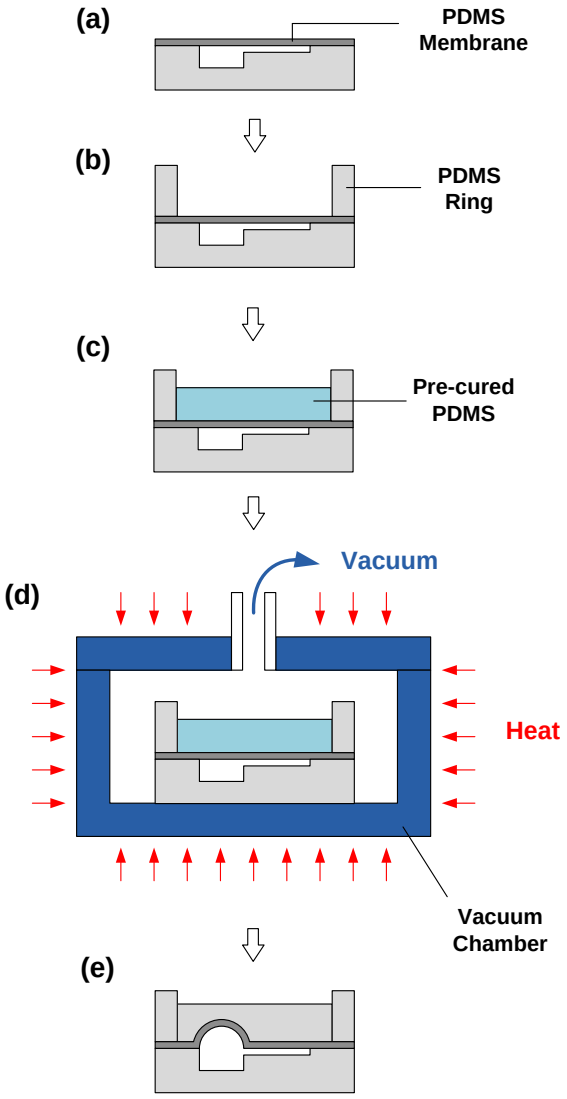

Figure D.1 Schematic of the vacuum expansion steps. (a) PDMS membrane attached to the PDMS replica. (b) PDMS wall structure attached. (c) Pre-cured PDMS poured inside the ring structure. (d) Whole device placed inside a vacuum chamber. Vacuum and heat were applied at the same time. (e) Vacuum expanded microfluidic channels resulting in raised cell aspiration channel.

PDMS membrane vacuum expansion procedure is as follows:

1. After oxygen plasma treatment, bond the ring shape structure made of PDMS on the PDMS membrane attached on the PDMS replica.
2. Mix PDMS (Sylgard® 184, Dow Corning, Inc., Midland, MI) in a 10 : 1 base : hardener ratio (w/w) and subsequently degas in a vacuum chamber for 20 minutes.
3. Gently pour the pre-cured PDMS inside the ring structure.
4. Place the whole device inside a vacuum chamber.
5. Apply vacuum (1E-2 torr = 1.3 Pa) and place the vacuum chamber inside the convection oven (140°C).
6. After 12 minutes, release vacuum and take out the device.

APPENDIX E

CELL CULTURE

HeLa cell line was maintained in accordance with the American Type Culture Collection (ATCC) guidelines as follows:

1. Remove and discard culture medium in 25 ml cell culture flask.
2. Rinse the cell layer with PBS twice.
3. Briefly rinse the cell layer with 0.25% (w/v) Trypsin- 0.53 mM EDTA solution to remove all traces of serum which contains trypsin inhibitor.
4. Add 500 µl of Trypsin-EDTA solution to flask and observe cells under an inverted microscope until cell layer is dispersed (usually within 3 to 5 minutes).
5. Add 5.0 ml of complete growth medium and aspirate cells by gently pipetting.
6. Move the cells into conical tube and centrifuge for 5 minutes at 800 rpm.
7. Remove and discard culture medium.
8. Add 2.0 ml of complete growth medium and disperse the cells by gently pipetting up and down several times.
9. Prepare new 25 ml cell culture flask and add 5 ml of growth medium inside.
10. Add appropriate aliquots of the cell suspension to the culture flask.
11. Incubate cultures at 37°C.

The procedure to make culture medium (500 μm) is as follows:

1. Thaw 50 ml of bovine serum (BS) and 10 ml of Pen/Step in water bath.
2. Pour 425 ml of DI water into a clean 500 ml beaker with stir bar.
3. Stir and add in 5 g of DMEM.
4. Add 1.755g D-glucose (Dextrose).
5. Add 0.75g of $NaHCO_3$ (Sodium bicarbonate).
6. Pour thawed 10ml of pen/step.
7. Make total volume 450ml by adding 15 ml of H_2O.
8. Add BS (50 ml) to the mixture.
9. Adjust pH to 7.3 using 2M HCl and NaOH.
10. Filter the medium using a 0.2 μm syringe filter (Acrodisk®, Pall Corp., USA) inside the bio-hood to sterilize.

APPENDIX F

PRESSURE DATA ACQUISITION

The voltage data from the pressure transducer (Omega) was acquired using LabVIEW™. VISA library was used for RS-232 serial cable communication. Figure F.1 and F.2 below show the front panel and block diagram of LabVIEW™ program respectively.

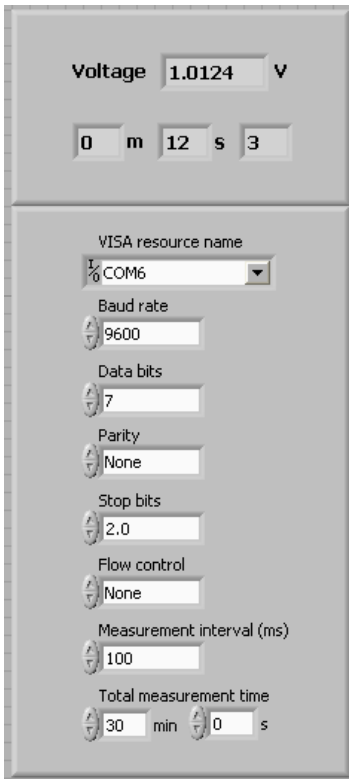

Figure F.1 LabVIEW™ front panel for data acquisition from the pressure transducer.

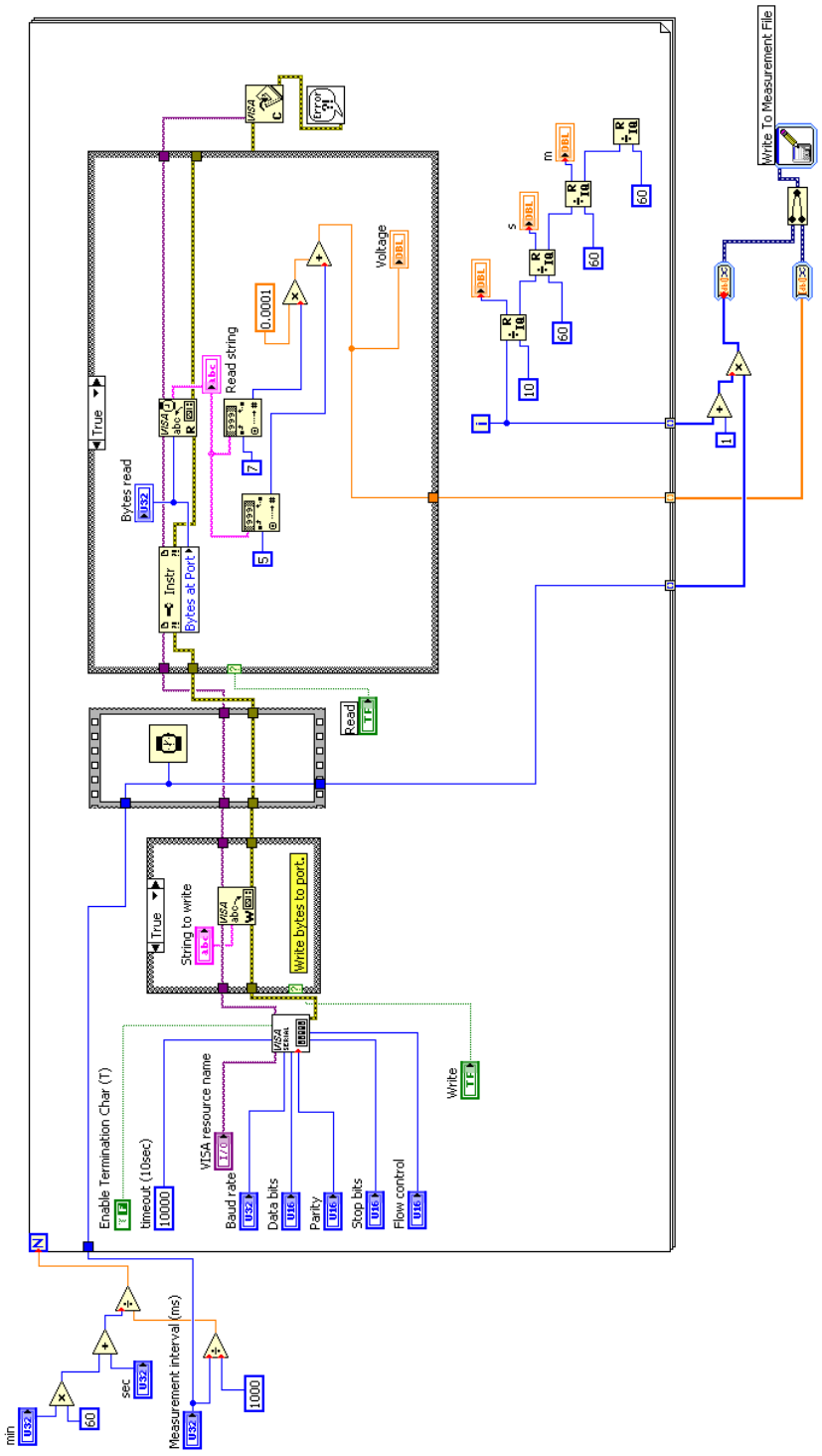

Figure F.2 LabVIEW™ block diagram for data acquisition from the pressure transducer.

VITA

Woosik Kim received his Bachelor of Science degree in Mechanical and Aerospace Engineering from Seoul National University in 2008. He entered the Department of Biomedical Engineering at Texas A&M University in September 2008 and received his Master of Science degree in August 2010. His research interests include microfluidics and miniaturized systems for cellular and molecular analyses.

Mr. Kim may be reached at 2739-6 Bangbae-2dong, Seocho-Gu, Seoul, Republic of Korea (South) 137-853. His email is kim.woosik@gmail.com.